An Acyl-CoA *N*-Acyltransferase Regulates Meristem Phase Change and Plant Architecture in Barley[1][OPEN]

Agatha Walla,[a,b,c] G. Wilma van Esse,[c,d] Gwendolyn K. Kirschner,[c,e] Ganggang Guo,[f] Annika Brünje,[g] Iris Finkemeier,[g] Rüdiger Simon,[c,e] and Maria von Korff[a,b,c,2,3]

[a]Institute of Plant Genetics, Heinrich-Heine-Universität Düsseldorf, 40225 Düsseldorf, Germany
[b]Department of Plant Breeding and Genetics, Max Planck Institute for Plant Breeding Research, 50829 Köln, Germany
[c]Cluster of Excellence on Plant Sciences "SMART Plants for Tomorrow's Needs", 40225 Düsseldorf, Germany
[d]Laboratory for Molecular Biology, Wageningen University and Research, 6708 PB Wageningen, The Netherlands
[e]Institute for Developmental Genetics, Heinrich-Heine-Universität Düsseldorf, 40255 Düsseldorf, Germany
[f]Institute of Crop Sciences, Chinese Academy of Agricultural Sciences (ICS-CAAS), Beijing 100081, China
[g]Plant Physiology, Institute of Plant Biology and Biotechnology, University of Münster, 48149 Münster, Germany

ORCID IDs: 0000-0003-4335-9454 (A.W.); 0000-0001-5012-2346 (G.W.v.E.); 0000-0002-3088-0315 (G.K.K.); 0000-0001-9970-5382 (G.G.); 0000-0002-8979-4606 (A.B.); 0000-0002-8972-4026 (I.F.); 0000-0002-1317-7716 (R.S.); 0000-0002-6816-586X (M.v.K.).

The modification of shoot architecture and increased investment into reproductive structures is key for crop improvement and is achieved through coordinated changes in the development and determinacy of different shoot meristems. A fundamental question is how the development of different shoot meristems is genetically coordinated to optimize the balance between vegetative and reproductive organs. Here we identify the *MANY NODED DWARF1* (*HvMND1*) gene as a major regulator of plant architecture in barley (*Hordeum vulgare*). The *mnd1.a* mutant displayed an extended vegetative program with increased phytomer, leaf, and tiller production but a reduction in the number and size of grains. The induction of vegetative structures continued even after the transition to reproductive growth, resulting in a marked increase in longevity. Using mapping by RNA sequencing, we found that the *HvMND1* gene encodes an acyl-CoA *N*-acyltransferase that is predominately expressed in developing axillary meristems and young inflorescences. Exploration of the expression network modulated by *HvMND1* revealed differential expression of the developmental microRNAs *miR156* and *miR172* and several key cell cycle and developmental genes. Our data suggest that *HvMND1* plays a significant role in the coordinated regulation of reproductive phase transitions, thereby promoting reproductive growth and whole plant senescence in barley.

Shoot architecture is a major determinant of plant function, diversification, and adaptation and is fundamentally important for the productivity of crop plants. It is largely defined by plant height, the arrangement and shape of leaves, branching (tillering) patterns, and inflorescence morphologies (Wang et al., 2018). These features are determined by the activity and fate of the shoot apical meristem (SAM), axillary meristems (AXMs), leaf meristems, and intercalary meristems (Teichmann and Muhr, 2015; McKim, 2019). During vegetative growth, the SAM initiates leaf primordia on its flanks, which later develop into leaves connected to the stem via a node. The leaf of cereal crops is an elongated structure consisting of the proximal sheath enclosing the meristem and culm, and the distal blade, which projects away from the stem axis to optimize light interception (Smith and Hake, 1992; Johnston et al., 2015; Digel et al., 2016; Conklin et al., 2019). In each leaf axil, typically a single AXM is initiated and forms, together with the leaf, node, and subtending internode, a phytomeric unit (McMaster, 2005; McSteen

[1]This work was funded by the Deutsche Forschungsgemeinschaft (DFG) under Germany's Excellence Strategy EXC-2048/1 (Project ID 390686111) and the National Natural Science Foundation of China (grant no. 31370032 to G.G.).
[2]Author for contact: maria.korff.schmising@hhu.de.
[3]Senior author.
The author responsible for distribution of materials integral to the findings presented in this article in accordance with the policy described in the Instructions for Authors (www.plantphysiol.org) is: Maria von Korff (maria.korff.schmising@hhu.de).
A.W., G.W.v.E., R.S., and M.v.K. conceived and designed the experiments; A.W. and G.W.v.E. performed the field experiments; A.W. conducted the phenotypic analyses; A.W. and G.W.v.E. conducted the RNA sequencing experiment and analyzed the data; G.G. contributed the characterization of the *mbd* mutant plant; A.W. performed allelism tests, gene resequencing, quantitative PCR experiments, and phylogenetic analysis; G.K.K. conducted in situ hybridization and protein localization experiments; A.B. and I.F. performed protein activity tests; and A.W. wrote the article with help from G.W.v.E. and M.v.K.
[OPEN]Articles can be viewed without a subscription.
www.plantphysiol.org/cgi/doi/10.1104/pp.20.00087

and Leyser, 2005). First, an AXM develops into an axillary bud (AB), which subsequently either remains dormant or grows out to form a primary tiller, including leaves, stem, inflorescence, and a succession of secondary tillers (Schmitz and Theres, 2005). In cereals, such as barley (*Hordeum vulgare*) and wheat (*Triticum aestivum*), only the ABs at basal unelongated internodes grow out and form tillers, while aerial ABs remain dormant (Oikawa and Kyozuka, 2009; Kebrom et al., 2013; Rossini et al., 2018).

Meristems adopt different identities during development, where meristem identity refers to the type of primordia produced (Poethig, 2010; Bartlett and Thompson, 2014; Bommert and Whipple, 2018; McKim et al., 2018). The SAM transitions from a vegetative meristem to an inflorescence meristem which then forms floral meristems on its flanks. Meristem determinacy regulates the number of primordia developed by each meristem and when and whether the meristem is eventually consumed in the production of primordia (Bartlett and Thompson, 2014). Developmental transitions typically take place in a highly regulated spatial and temporal context, with clear directionality (Keyte and Smith, 2014). However, meristem reversion may also occur, where, for example, floral meristems revert to vegetative branches (Tooke et al., 2005; Trevaskis et al., 2007; Müller-Xing et al., 2014; Asbe et al., 2015; Li et al., 2019). Consequently, shoot architecture is dependent on the initiation of meristems, the timing of identity transitions, and meristem determinacy, which denotes when a meristem ceases to produce lateral organs and terminally differentiates, i.e. into flowers.

The initiation and development of the different shoot meristems need to be coordinated to optimize the allocation of limited resources to the different plant organs and thus optimize plant performance and fitness (Liller et al., 2015). Generally, plants follow different life strategies. They either invest more in vegetative structures, maintaining undifferentiated meristems for extended growth and survival, or they invest more in seed production, typically followed by whole plant senescence and death (Albani and Coupland, 2010). Perennial plants that live over many seasons versus annual plants that only reproduce once and then die represent extremes of the spectrum. Trade-offs or linkage between the development and fate of different shoot organs also controls productivity in annual crop plants (Sadras, 2007; Guo et al., 2018). In cereal crops, negative correlations between tiller (spike) number, grain number, and grain size have hampered the genetic improvement of overall yield (Liller et al., 2015). Consequently, a fundamental question is how the activity and development of different shoot meristems are coordinately regulated. Elucidating the underlying genes and regulatory networks would offer valuable guidance for plant breeding practices and provide genetic tools for the dissection of linked traits.

The highly regulated progression through developmental phase changes and coordinated development of different plant meristems suggests the presence of master regulators that trigger critical developmental transitions simultaneously in several different tissues. The conserved plant microRNAs miR156 and miR172 have been identified as such key regulators of phase changes in plant meristems. Overexpression of *miR156* or *miR172* causes strong pleiotropic phenotypes such as increased tillering, aerial branching and defective spike branching in wheat, maize (*Zea mays*), and rice (*Oryza sativa*; Xie et al., 2006; Chuck et al., 2007; Zhu et al., 2009; Liu et al., 2017). The identification of further regulators and genetic dissection of their activity and function in different plant meristems of cereal crops is important for precise manipulation of meristem identity and activity during plant development. While the control of phase change and its profound effects on shoot architecture have been studied in the grass crops maize and rice (Poethig, 1988; Kyozuka et al., 2014; Hibara et al., 2016), much less is known about the coordinated control of different shoot meristems, the timing of meristem phase changes, and investment in vegetative versus reproductive plant structures in the temperate cereals wheat and barley.

The discovery of genes and regulatory networks underlying shoot architecture in barley is facilitated by the large collection of developmental mutants, many of which have been backcrossed to cv Bowman to generate near isogenic lines (NILs; Bossinger et al., 1992; Franckowiak et al., 1996). This mutant collection includes many termed "*many noded dwarf*" (*mnd*) that have a short plant stature and increased node numbers, tillering, and vegetative biomass (Harlan and Pope, 1922; Gustafsson, 1947). These *mnd* mutants represent a valuable resource for detecting genes that control shoot branching and vegetative versus reproductive growth. Among the *mnd* mutants, only the gene underlying the *mnd4/6* mutation has been cloned so far, and it encodes a cytochrome p450 protein, an ortholog of the rice *PLASTOCHRON1* (*PLA1*) gene (Mascher et al., 2014).

Here we characterized the pleiotropic phenotype of allelic barley high-tillering mutant plants. We demonstrated that these mutants exhibit a delay in the transition to reproductive growth that is linked to a strong increase in the number of leaves and tillers but an overall decrease in grain yield. Outgrowth of ABs at aerial nodes, floral reversion, and bract development indicated reduced apical dominance in the *mnd1* mutant plants. Mapping by RNA sequencing revealed that the *HvMND1* locus encodes an acyl-CoA *N*-acyltransferase. Expression analysis demonstrated that this gene is specifically transcribed in the AXMs and SAMs and controls the expression of key developmental genes and genes of the cell cycle machinery. Our data suggest that *HvMND1* plays a significant role in the coordinated regulation of phase transition, thereby promoting reproductive versus vegetative growth.

RESULTS

MND1 Regulates Shoot Branching and Inflorescence Development

We investigated the macro- and microscopic phenotypes of the *mnd1.a* mutant, which was originally

identified as a high-tillering mutant in a mixed field of wheat and barley (Harlan and Pope, 1922). We scored plant height, flowering time, and yield in the original mutant line in cv Mesa, where the *mnd1.a* mutation had occurred spontaneously, and its backcross-derived NILs in cv Bowman as well as in the parental lines in outdoor experiments over two consecutive years. For simplicity, we will hereafter refer to the mutants as *mnd1.a* (M) for the original mutant line and *mnd1.a* for the backcross-derived NIL in cv Bowman. The *mnd1.a* mutants in both backgrounds were stunted and exhibited a high-tillering phenotype (Fig. 1, A–C) in agreement with previous reports (Harlan and Pope, 1922; Bregitzer et al., 2014). Moreover, both *mnd1.a* mutant lines flowered significantly later than the corresponding wild-type plants, with wild-type cultivars and mutant lines flowering ~73 d and 86 d or more, respectively, after seedling emergence (Fig. 1D). Although the mutants were 40% shorter than the corresponding wild types, they nevertheless produced significantly more vegetative biomass (Fig. 1E). In contrast, the generative biomass per plant and the thousand grain weight (TGW) were lower in both mutants (Fig. 1, F and G) due to 20% smaller kernels caused by a decrease in grain width and length (Supplemental Fig. S1, B–D). Additionally, the spike length and number of grains per spike were significantly lower in the mutants compared to the corresponding wild-type plants (Fig. 1H; Supplemental Fig. S1A). Consequently, the *mnd1.a* mutation increased the vegetative biomass but reduced the generative biomass given the smaller grain size and grain number.

Since the *mnd1.a* mutants exhibited a delay in flowering time, we further investigated the development of the main SAM in cv Bowman and the derived introgression line under inductive long-day (LD) conditions according to the Waddington scale (Fig. 2A). The Waddington scale is a quantitative scale for barley and wheat development based on the morphogenesis of the shoot apex and the carpel of its most advanced flower (Waddington et al., 1983). The emergence of the first spikelet primordia on the shoot apex at the double ridge stage (W2.0) specifies a reproductive SAM. The first floral organ primordia differentiate and stem elongation starts at the stamen primordium stage (W3.5). Anthesis and pollination of the most advanced floret occur at the last stage of the Waddington scale (W10.0). In the *mnd1.a* mutant, spikelet initiation and inflorescence development were delayed compared to those of cv Bowman (Fig. 2A). This delay in spikelet initiation was linked to an increase in the number of leaves on the main shoot of the mutant (Fig. 2B). Five weeks after emergence (WAE), no further leaves appeared on the main shoot in cv Bowman, and the plants flowered with approximately six leaves. In contrast, the *mnd1.a* mutant showed a steady increase in leaf number throughout development until 9 WAE, when the experiment was terminated. The production of supernumerary leaves on the main shoot was associated with an increase in the number of elongated internodes (Supplemental Fig. S2A). Although *mnd1.a* mutant plants initiated leaf primordia for a longer period, the plastochron, which is the leaf initiation rate, was unchanged between cv Bowman and *mnd1.a* (Supplemental Table S1). However, the appearance of successive leaves on the main culm was faster in the mutant (Fig. 2B). The time between the visual appearance of two successive leaf tips was 5.6 d in cv Bowman plants, whereas *mnd1.a* mutant plants developed two successive leaves in only 2.2 d (Supplemental Table S1). This demonstrates that the *mnd1.a* mutation caused a shorter phyllochron and an increase in phytomers due to the prolonged vegetative development. In addition, lengths and widths of the leaf blades and lengths of the leaf sheaths were significantly reduced in the mutant, as shown for the first three fully developed leaves (Fig. 2, C and D; Supplemental Fig. S2C). The short leaf phenotype coincided with an earlier termination of leaf growth of the first leaf (L1) in the mutant compared to L1 in cv Bowman (Supplemental Fig. S2B). To determine whether the shorter leaves in the mutant were caused by a change in cell elongation or proliferation, we examined the adaxial epidermal cells of L1 in both genotypes. No differences were found for average cell length (Fig. 2E; Supplemental Fig. S2, D and E), but cells located over veins next to sclerenchyma and lateral cells were enlarged in the mutant (Supplemental Fig. S2, D and E). Consequently, the shorter leaves in the mutant were not caused by a reduction in cell size, but resulted from a lower cell number.

To determine whether the higher tiller number was linked to the development of additional leaves (Fig. 2, B and G), we dissected tiller development at defined developmental stages in the wild-type and mutant plants. Significantly more tillers were already observed on the main shoot in the *mnd1.a* mutant compared to cv Bowman at the glume primordium stage (W3.0; Fig. 2F). At the awn primordium stage (W5.0), cv Bowman had developed two to three tillers, whereas the main shoots of the *mnd1.a* mutant had established >40. We then analyzed the pattern of AB formation at the main stem at three different stages of early development (Fig. 3A). For this purpose, the leaf axil of each leaf >0.3 mm on the main culm was examined for the presence or absence of an AB or tiller. We classified ABs as young when they were surrounded by only the first leaf or mature when they were enclosed in more than one leaf and secondary ABs had potentially formed. As bud outgrowth progressed, we further classified tillers into young tillers with only one visible shoot and mature tillers if secondary side shoots were apparent. At 1 WAE, one to two more leaves were produced in the *mnd1.a* mutant compared to cv Bowman. However, *mnd1.a* and wild-type plants produced the same relative number of ABs per leaf axil (0.6 and 0.6 at 1 WAE, 0.4 and 0.5 at 3 WAE, and 0.5 and 0.5 at 5 WAE for cv Bowman and *mnd1.a*, respectively), but buds were further developed in *mnd1.a* than in cv Bowman. At 3 WAE, cv Bowman plants did not form further leaves on the main culm due to the initiation of spikelet primordia

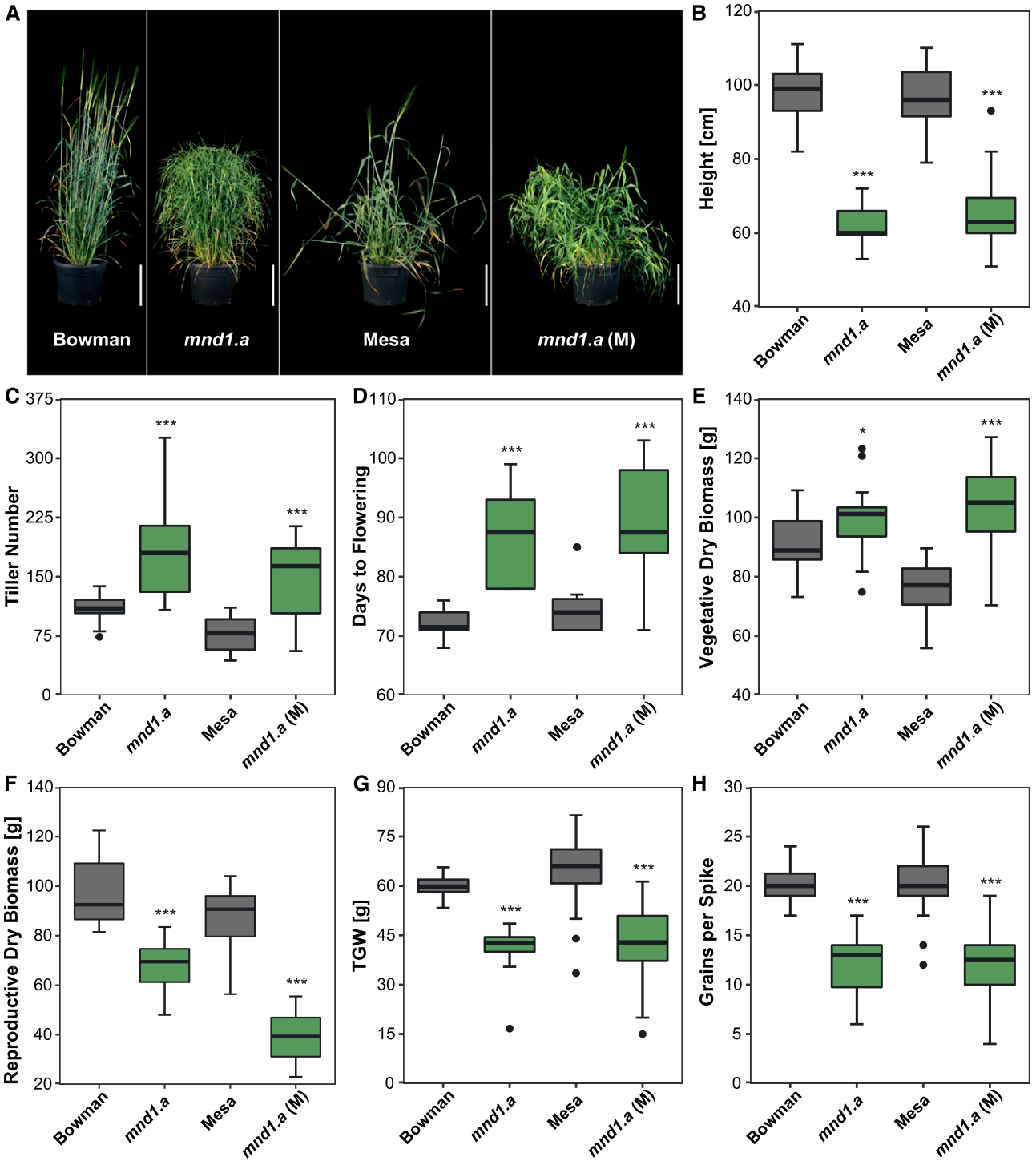

Figure 1. Phenotypic characteristics of adult *mnd1.a* mutants grown under outdoor conditions. A, Morphology and plant architecture of the spontaneous *mnd1.a* mutant in cv Mesa [*mnd1.a* (M)] and its backcross-derived NIL in cv Bowman (*mnd1.a*). Scale bars = 25 cm. B and C, Comparison of plant height (B) and tiller number (C) between the *mnd1.a* mutants and the corresponding parents representing each genetic background. D, Flowering time in days until the appearance of the first awns from the flag leaves. E and F, Vegetative (E) and reproductive (F) biomass per plant after senescence and an additional drying period. G and H, TGW (G) and grains per spike (H) for each genotype. Data were obtained from outdoor trials in the consecutive years 2014 and 2015 ($n = 10–40$). Box plots show the median and interquartile range, error bars show the 10th and 90th percentiles, and dots are outliers. Statistical significance was assessed for each mutant and the corresponding genetic background cultivar by a two-tailed unpaired Student's *t* test (*$P < 0.05$, **$P < 0.01$, and ***$P < 0.001$).

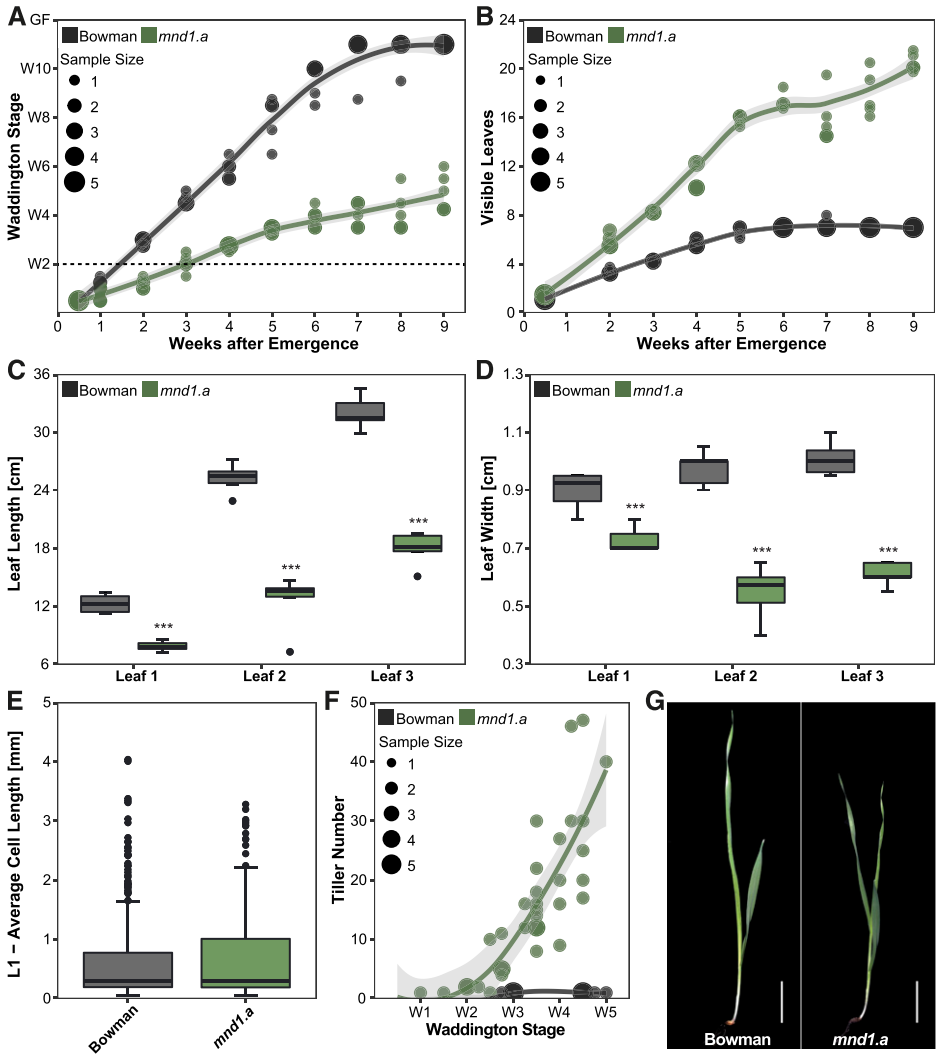

Figure 2. Influence of the *mnd1.a* locus on plant development. A, Development of the main SAM under LD conditions, reported in Waddington stages. The dotted line at W2.0 marks the stage of spikelet primordia initiation. GF, Grain filling. B, Number of visible leaves developed on the main shoot. C and D, Leaf length (C) and width (D) of the first three fully developed leaves. Leaf sizes were measured at the longest/broadest position ($n \geq 16$). E, Average cell size of all cell types ($n = 350$ cells) in the adaxial epidermis of the first fully developed leaf (L1) measured according to the method of Wenzel et al. (1997). F, Number of tillers in *mnd1.a* and cv Bowman according to the SAM developmental stage up to W5.0. Gray areas around fitted curves indicate the 95% confidence interval. Statistical significance was assessed by a two-tailed unpaired Student's *t* test (*$P < 0.05$, **$P < 0.01$, and ***$P < 0.001$). G, Seedling morphology of cv Bowman and *mnd1.a* at 10 DAE grown in a short-day climate chamber. Scale bars = 2 cm.

and termination of the vegetative program. In contrast, the *mnd1.a* mutant continued to form leaves or leaf-like structures until 5 WAE, when spikelets were initiated (Fig. 3A). However, the ratio of AB to leaf number remained the same at 3 WAE for the mutant and wild type. This indicated that the high number of ABs in the *mnd1.a* mutant was a consequence of the increased leaf number. Moreover, AB formation continued during inflorescence development and was observed at aerial nodes in the *mnd1.a* mutant, whereas leaf axils at elongated internodes remained without AB formation in cv Bowman (Fig. 3, A and B). In *mnd1.a* plants, ABs formed at all elongated internodes, with the exception of a restricted region approximately between nodes 12 and 22 (Fig. 3, A and B). In addition, young ABs formed below and at the base of the inflorescence. The development of such aerial ABs was observed starting at early reproductive stages of inflorescence development, after the reproductive transition (W3.0–W3.5; Fig. 3C). The morphology of the young aerial ABs was identical to that of ABs at the plant base, with leaf primordia enclosing a vegetative shoot meristem. Aerial ABs initiated leaves, underwent stem elongation, developed inflorescences, and eventually set kernels (Fig. 3, C and D). We further observed the formation of nodal root buds at nodes where aerial ABs had formed (Supplemental Fig. S4D). In a separate experiment we determined the duration of tillering of the *mnd1.a* mutant under controlled conditions. While Bowman plants underwent whole-plant senescence within 3 months, the *mnd1.a* mutant plants continued to generate new leaves and tillers at the base of senescent tillers for >12 months, when the experiment was stopped (Supplemental Fig. S4, A–C). Consequently, the *mnd1.a* locus affected not only tiller number but also duration of tillering and therefore longevity and whole-plant senescence in barley.

To determine the origin of the ABs at the base of inflorescences in the *mnd1.a* mutant, we compared the morphology of developing inflorescences in wild-type and mutant plants at the glume primordium stage (W3.0), the stamen primordium stage (W3.5), and the awn primordium stage (W5.0) by scanning electron microscopy. We found that the aerial ABs at the

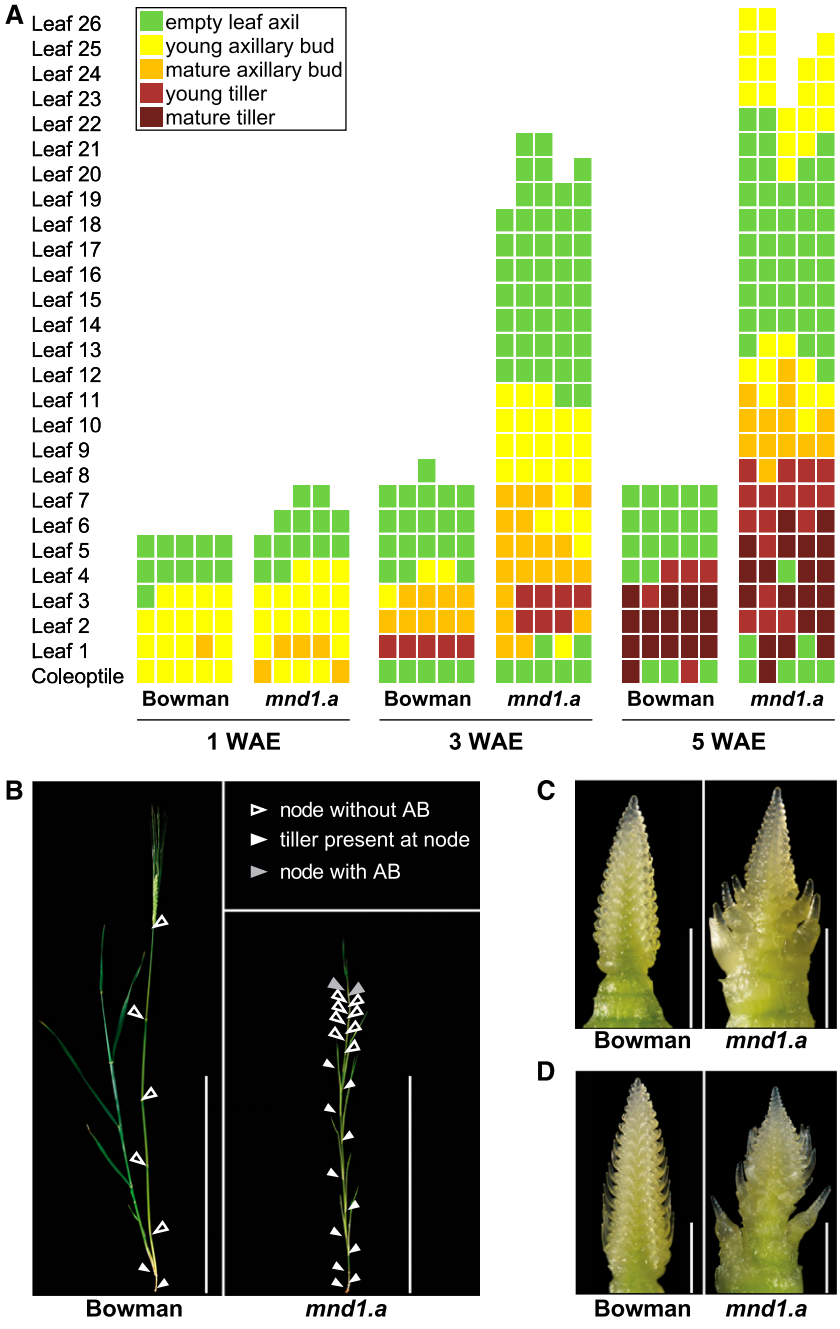

Figure 3. Axillary bud initiation pattern in cv Bowman and *mnd1.a* mutants. A, Schematic representation of AB formation at 1, 3, and 5 WAE in cv Bowman and *mnd1.a* mutants. Leaf axils were examined under a binocular microscope. Each column represents the main stem of a single plant of the respective genotype, and each square represents an individual leaf axil. The bottom row represents the axil of the coleoptile, whereas axils of progressively younger leaves are stacked on top, with leaf 1 as the oldest leaf. The absence of AB formation is coded in green, and the presence of ABs is shown in yellow to dark red depending on the developmental status of the axillary shoot. B, Internode patterning on the main stem and AB and tiller positions in cv Bowman and *mnd1.a* mutants at 7 WAE. Node positions along the main stem are indicated with triangles. Triangle color and shape indicate the presence or absence of ABs or tillers at the corresponding node. The uppermost node in cv Bowman ends the peduncle. C, Inflorescence phenotype of *mnd1.a* mutants at W3.5. D, Inflorescence phenotype of *mnd1.a* mutants at W5.0. Leaves around the SAM and ABs were removed for visualization of the phenotype. Scale bars = 30 cm (B) and 1 mm (C and D).

inflorescence base were present at all analyzed stages in the *mnd1.a* mutant (Fig. 4A). These branch meristem-like structures were still vegetative at the stamen primordium stage but initiated spikelet primordia when the inflorescence had transitioned to the awn primordium stage. In particular, the development of the branch meristem-like organs coincided with a disturbed bract suppression in *mnd1.a* inflorescences. In cv Bowman, bract growth at the collar and rachis nodes was suppressed. However, in the *mnd1.a* mutant, leaf-like structures termed floral bracts and known as third outer glumes (Houston et al., 2012) were subtending the triple spikelet primordia at the rachis nodes and coincided with the reversion of the triple spikelet meristem to a branch meristem (Fig. 4A). Eventually, bracts at the basal rachis nodes expanded and were able to enclose the spike, whereas bracts at the upper rachis nodes were not visible in maturing *mnd1.a* spikes (Fig. 4B). Moreover, the rachis internodes were elongated at the location of bract outgrowth, causing the *mnd1.a* spikes to adopt an accordion-shaped morphology (Fig. 4B). Cv Bowman and cv Mesa are two-rowed barley cultivars where only the central spikelet meristem develops a flower and grain, while the floral organ development of lateral spikelets is impaired, resulting in infertility. However, in the *mnd1.a* mutant, the

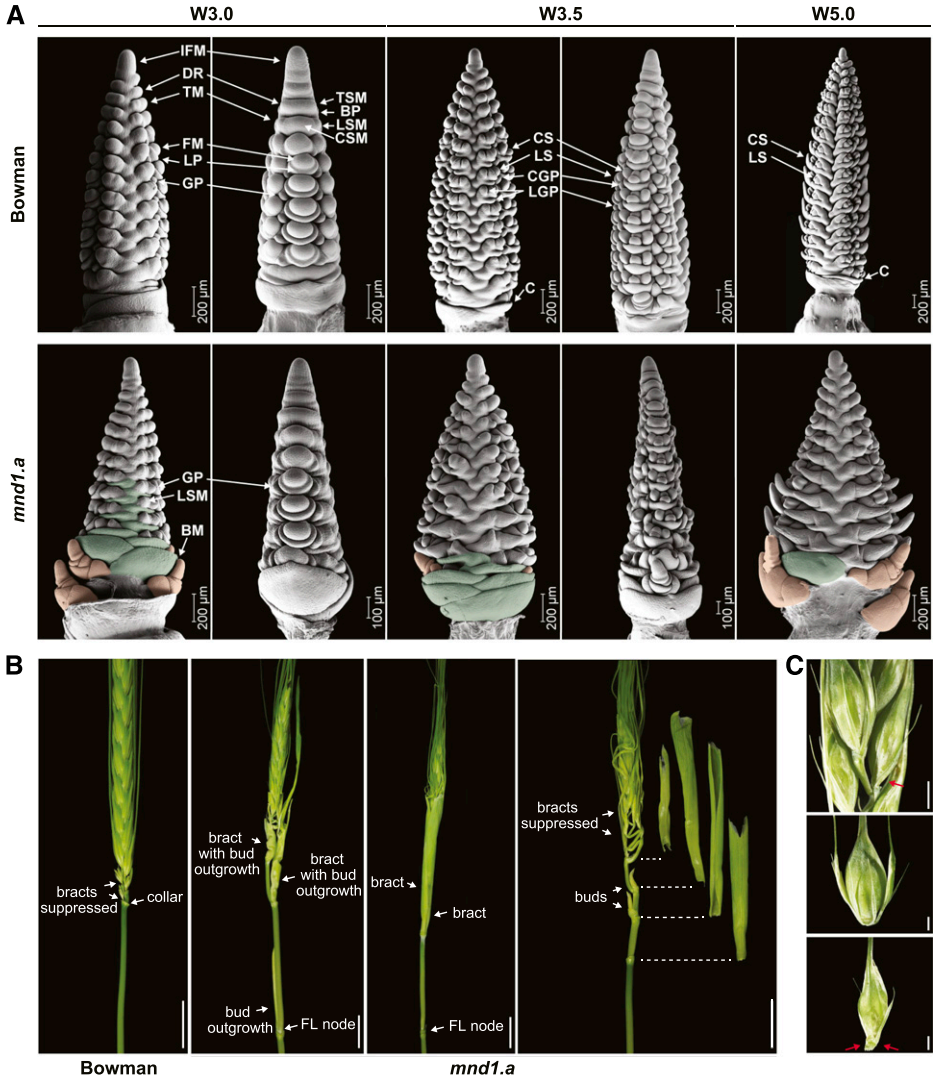

Figure 4. Wild-type and *mnd1.a* mutant inflorescence development. A, Scanning electron microscopy images of developing inflorescences from the glume primordium stage (W3.0) to the stage of stamen primordia initiation (W3.5) to the awn primordium stage (W5.0) in cv Bowman (top), and main inflorescences in the *mnd1.a* mutant investigated at comparable developmental stages (bottom). Subtending bracts at *mnd1.a* inflorescence bases were removed to expose the spikelet meristem reversion to branch meristem-like structures. In frontal-angle images, exemplary outgrowing bracts were highlighted in green and branch meristem-like structures in orange. Lateral-angle images of apices were not colored. IFM, Inflorescence meristem; DR, double ridge; TM, triple mound; TSM, triple spikelet meristem; BP, bract primordium; LSM, lateral spikelet meristem; CSM, central spikelet primordium; FM, floral meristem; LP, lemma primordium; GP, glume primordium; CS, central spikelet; LS: lateral spikelet; CGP, central glume primordium; LGP, lateral glume primordia; C, collar; BM, branch meristem-like. B, Bract outgrowth phenotype observed in *mnd1.a* inflorescences. Arrows indicate rudimentary, suppressed bracts and collar in the wild-type cv Bowman inflorescence and outgrown and suppressed bracts, aerial buds, and flag leaf node in *mnd1.a* inflorescences. No collar formed in the *mnd1.a* mutants, but a bract was present instead. FL, Flag leaf. Scale bars = 1 cm. C, Lateral floret presence/absence phenotype of *mnd1.a* mutants. Top, Basal part of a *mnd1.a* inflorescence. Middle and bottom: Spikelets detached from basal *mnd1.a* inflorescences. Red arrows indicate absence of lateral florets. Scale bars = 1 mm.

development of these lateral spikelet structures was impaired. Some lateral floral meristems failed to initiate after the differentiation of the corresponding lateral glume primordia, especially at the basal region of the inflorescence where bracts grew out (Fig. 4C). In addition to branches at the base of the *mnd1.a* inflorescences, we also observed the occasional formation of ABs in the axils of flag leaves (Fig. 4B). Consequently, reduced bract suppression at lower rachis nodes, reversion of spikelet meristems to branch meristem-like organs, and initiation of ABs in flag leaf axils contributed to a highly branched shoot architecture in the *mnd1.a* mutant. Moreover, we observed differences in inflorescence length and spikelet numbers between the *mnd1.a*

mutant and cv Bowman (Supplemental Fig. S3, A and B). The length of *mnd1.a* inflorescences was comparable to that of wild-type inflorescences at spikelet initiation (W2.0). During further development, inflorescence growth (W3.5–W6.0) and rate of spikelet initiation were reduced in *mnd1.a* compared to the wild type. At W6.0, cv Bowman plants had initiated an average of 34 spikelets, compared to 24 in *mnd1.a* mutant plants. The lower number of spikelets in the *mnd1.a* mutant was also caused by the reversion to branch meristem-like organs at the basis of inflorescences, as described above (Supplemental Fig. S1A).

Taken together, the *mnd1.a* mutant produced more leaves and tillers than did wild-type plants due to (1) a longer vegetative growth period, (2) faster leaf outgrowth, (3) formation of ABs at aerial nodes, and (4) reduced bract suppression and floral reversion. Consequently, the mutation underlying the *mnd1.a* locus coordinates the timing of developmental programs and thus is a major pleiotropic modifier of barley shoot and inflorescence architecture.

Identification of the Gene Underlying the *mnd1.a* Locus

To map the gene, determine the polymorphism underlying the *mnd1.a* mutation, and identify potential molecular targets of the gene in developing inflorescences, we performed a RNA sequencing experiment as previously described (van Esse et al., 2017). We sequenced total RNA from main inflorescences of the backcross-derived *mnd1.a* mutant and cv Bowman at three developmental stages: spikelet initiation (W2.0), the stamen primordium stage (W3.5), and after awn primordia had emerged and started to elongate (W5.0). Furthermore, RNA was extracted and sequenced from leaf-enriched SAM samples at W1.0 of the original parent cv Mesa for comparison of sequence variation originating from this line. To identify polymorphisms in the sequenced genotypes, all reads from one genotype were pooled regardless of the developmental stage of the SAM, enabling better coverage of expressed transcripts and ultimately more support for variant identification. We compared the variants identified for cv Bowman and the *mnd1.a* mutant and found 261 polymorphic alleles. By mapping the 261 alleles to the ordered sequence of the barley reference genome (Mascher et al., 2017), we identified two introgression regions on chromosomes 2H and 7H in the backcross-derived *mnd1.a* mutant (Fig. 5, A and B), corroborating previous reports (Druka et al., 2011). To narrow down the list of 261 candidate genes, polymorphisms shared between the *mnd1.a* introgression line, the original parent cv Mesa, and reference cv Morex were excluded as candidates for the *mnd1.a* phenotype, revealing a total of 56 genes with unique mutations to *mnd1.a* (Fig. 5B). Among these, 32 alleles carried nonsynonymous mutations, 10 mutations were located in a conserved domain, and only two were predicted to be functionally important according to the PROVEAN score (cutoff of −2.5; Supplemental Table S2; Choi and Chan, 2015). The candidate gene located within the introgression region on chromosome 2H encodes a ribosomal L12 family protein (HORVU2Hr1G029240), whereas the candidate gene located within the introgression on chromosome 7H encodes an acyl-CoA *N*-acyltransferase superfamily protein (HORVU7Hr1G113480.3). The ribosomal L12 family protein carried an amino acid substitution in its conserved ribosomal protein L7/L12 domain (Supplemental Table S2), and the acyl-CoA *N*-acyltransferase superfamily protein carried a frameshift mutation due to an 8-bp insertion in the *mnd1.a* mutant allele (Fig. 5C; Supplemental Table S2). This insertion was located in the second of three exons at the beginning of the conserved *N*-acetyltransferase domain, leading to a mistranslation and a premature stop codon. To confirm the mutations obtained from the RNA sequencing reads, we sequenced both candidate genes in cv Bowman, cv Mesa, and the backcross-derived and original *mnd1.a* mutant lines (Supplemental Table S3). The 8-bp insertion in the acyl-CoA *N*-acyltransferase was detected in both *mnd1.a* mutant lines but was absent from the parental cultivars. However, we detected the candidate polymorphism in the ribosomal L12 family protein only in the backcross-derived *mnd1.a* line and not in the original *mnd1.a* mutant or the parental cultivars. Because the ribosomal L12 family protein polymorphism was not shared between both *mnd1.a* mutant lines, we selected the acyl-CoA *N*-acyltransferase as the candidate gene underlying the *mnd1.a* locus. To confirm the candidate gene, we made use of two independent mutant lines, *many branched* (*mbd*) in the background of cv ZOH (Zhang, 1997) and MHOR198 in the background of cv HOR3069. Both mutants were late flowering and produced aerial branches like the *mnd1.a* mutant (Supplemental Figs. S5 and S6; Supplemental Tables S4 and S5). We performed complementation experiments by crossing *mnd1.a* that carried a recessive mutation with either the *mbd* or MHOR198 mutant (Harlan and Pope, 1922; Hor, 1924). Compared to the parental wild-type cultivars, the resulting F1 progeny were late flowering and characterized by prolific tiller production, more nodes, and the presence of aerial branches (Supplemental Figs. S5 and S6; Supplemental Tables S4 and S5). Consequently, the *mbd* and MHOR198 mutants were identified as allelic to *mnd1.a.* Sequencing the two candidate genes in the *mbd* and the MHOR198 lines revealed no mutation in the L12 family protein, while the candidate acyl-CoA *N*-acyltransferase gene was deleted in *mbd* and carried a 2-bp insertion in the second exon, causing a frame-shift mutation in MHOR198 (Supplemental Table S3). We therefore concluded that the *mnd1.a* phenotype is caused by a loss-of-function mutation in the acyl-CoA *N*-acyltransferase in the three allelic *mnd1.a* mutant lines.

The maximum-likelihood tree of *HvMND1* homologs defined a MND1-family clade comprising the barley *MND1* gene along with 57 MND1-like proteins from

nine monocots, nine dicots, and the spikemoss *Selaginella moellendorffii*. The MND-like proteins from the angiosperms fell into the two monophyletic clades of dicots and monocots. The tree topology indicated a series of independent duplications of the *MND1*-like genes within the Poaceae clade (Supplemental Fig. S7). In barley, a recent duplication event was observed resulting in HvMND1 and its closest paralog HORVU5Hr1G071620.1 located on chromosome 5H. The previously identified GCN5-related *N*-acetyltransferase-like protein OsglHAT1 (LOC_Os06g44100.1; Song et al., 2015) is the closest homolog of HvMND1 in rice (74.81% amino acid identity), and the encoding gene is located in a syntenic region on chromosome 6 (Mayer et al., 2011). In the Arabidopsis (*Arabidopsis thaliana*) genus, we identified three homologs of HvMND1, all acyl-CoA *N*-acyltransferase (NAT) superfamily proteins, including the ethylene response gene *HOOKLESS1* (*HLS1*), which is essential for seedling growth (Lehman et al., 1996). We further investigated the natural diversity of *HvMND1* using resequencing data of 91 wild barley, 137 landrace, and 91 research and elite breeding lines (Russell et al., 2016). Only polymorphisms in the coding sequence (CDS) of *HvMND1* were extracted and aligned together with corresponding sequences from cv Mesa and the *mnd1.a* allele (Supplemental Dataset 1). The subsequent haplotype analysis resulted in 11 haplotypes (excluding cv Mesa and the *mnd1.a* allele; Supplemental Fig. S8). The majority of analyzed accessions carried one of two main haplotypes, whereas the remaining genotypes belonged to nine minor haplotypes (Supplemental Fig. S8, Supplemental Table S6). Among the polymorphic sites underlying the haplotype network, only six were nonsynonymous changes. Variant-effect analysis using PROVEAN (Choi and Chan, 2015) predicted neutral effects on protein function for all nonsynonymous changes except one (single amino acid substitution V92A). However, when we grew plants that fell into this haplotype, we did not observe any phenotype resembling the *mnd1.a* mutant. The *mnd1.a* allele itself and the related Mesa allele were derived from one of the major haplotypes. Overall, we observed a high sequence conservation for *HvMND1*, in agreement with its function as a major regulator of barley development.

HvMND1 Transcript Localization

We investigated the localization of *HvMND1* transcripts in cv Bowman SAMs, inflorescences, and crown tissue by mRNA in situ hybridization. We observed distinct *HvMND1* expression foci at the abaxial base of

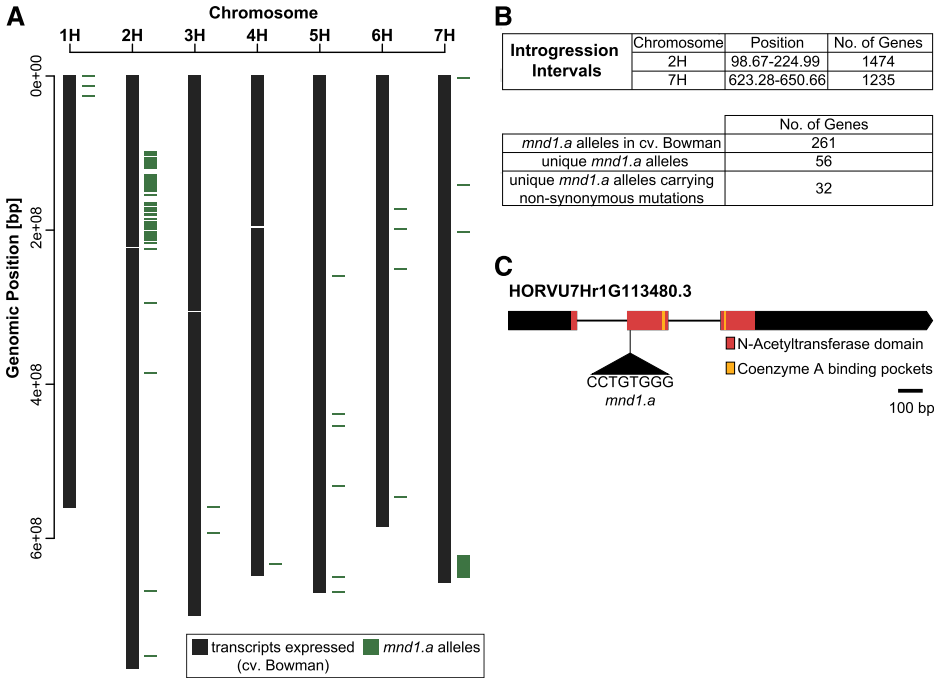

Figure 5. Introgression mapping and candidate gene selection for the *mnd1.a* locus. A, Visualization of the *mnd1.a* introgressions introduced to the reciprocal backcross parent cv Bowman. Black lines represent genes expressed in cv Bowman in the transcriptome data set with a coverage of least four reads. Alleles originating from the primary *mnd1.a* mutant in cv Mesa were identified through variant calling on the transcriptome sequencing data and mapped to the barley genome according to the physical distance. B, Overview of the introgression intervals of the backcross-derived *mnd1.a* mutant line and reduction of candidate genes through filtering steps. C, Intron-exon organization of the candidate gene underlying the *mnd1.a* locus. The gene contains three exons (boxes) encoding a conserved *N*-acetyltransferase motif with two coenzyme A binding pockets. The *mnd1.a* allele contains an insertion of 8 bp in the second exon.

young developing leaves, and this persisted through all investigated stages of vegetative (W1.0–W1.5) and reproductive (W2.0, W3.5, and W5) SAM development (Fig. 6, A–D). This expression pattern was also observed in young ABs, where *HvMND1* transcripts localized to the abaxial base of young leaves enclosing the AXM (Fig. 6B). In addition, we detected *HvMND1* expression in SAMs undergoing the transition from vegetative to reproductive development (W2.0), with *HvMND1* transcripts localizing broadly to the vasculature of the developing inflorescence, but not in vegetative SAMs or in later stages of inflorescence development. We verified the localization of *HvMND1* expression in cv ZOH and tested for expression in the derived deletion mutant *mbd*, as well as in the cv Bowman-derived *mnd1.a* mutant line at spikelet initiation (W2.0). The localization of *HvMND1* mRNA was comparable between the *mbd* parental background cv ZOH and cv Bowman (Supplemental Fig. S9). *HvMND1* expression was not detected in inflorescences of the *mnd1.a* and *mbd* mutants at W2.0 (Supplemental Fig. S9, G and H). Furthermore, cellular localization of HvMND1 was investigated using infiltrated *Nicotiana benthamiana* leaves transiently expressing HvMND1 fused to GFP. We found that HvMND1 localized in the nucleus and colocalized with the plasma membrane of the *N. benthamiana* cells (Supplemental Fig. S9I). To assess whether HvMND1 is a functional acetyltransferase, we compared proteome-wide Lys acetylation in young inflorescences (W3.5) of cv Bowman and the loss-of-function mutant *mnd1.a* by immunoblot analysis (Supplemental Fig. S10). We did not detect any differences in the amount or abundance of Lys-acetylated proteins, including histones, indicating that the putative acetyltransferase activity of HvMND1 might be very specific to a subset of cells and/or target proteins, as suggested by the very localized expression of *HvMND1* in the inflorescence. The spatial and temporal expression of *HvMND1* was further investigated by reverse transcription quantitative PCR (RT-qPCR) in different plant tissues of cv Bowman and in a developmental series of SAMs in cv ZOH. In cv Bowman, *HvMND1* expression was detected in the crown tissue of 3-d-old seedlings and in the nodes of the uppermost elongated internode segment of plants at W3.5 (Supplemental Fig. S11A). In the roots of 3-d-old seedlings, *HvMND1* expression levels were close to the detection limit, whereas *HvMND1* was not expressed in fully expanded leaves. Moreover, *HvMND1* expression was detected in the leaf-enriched SAM samples of cv ZOH at all sampled stages, from vegetative SAMs to young developing inflorescences (Supplemental Fig. S11B). In summary, *HvMND1* was expressed in leaf axils at AXM initiation zones close to the SAM and in the vasculature of SAMs undergoing floral transition but was absent or showed low expression in other plant organs.

Transcriptional Profiling by RNA Sequencing

To determine the molecular function and potential target genes of *HvMND1*, we investigated transcriptional changes in developing inflorescences in cv Bowman and the backcross-derived *mnd1.a* mutant. For this purpose, the whole transcriptome data set used for candidate gene identification was screened for transcripts that were differentially expressed between the genotypes in leaf-enriched inflorescence tissues at early reproductive developmental stages (W2.0, W3.5, and W5.0). Principal component analysis of all expressed transcripts in cv Bowman and the *mnd1.a* mutant revealed that the developmental stage explained most of the variance (principal component [PC] 1; 34% of the total variance) followed by the genotype (PC2; 11.73% of the total variance; Supplemental Fig. S12A). A hierarchical cluster analysis of differentially expressed transcripts (DETs) showed that DETs at W2.0 grouped separately from those at W3.5 and W5.0, which were more similar in terms of their expression profile (Supplemental Fig. S12B). Furthermore, the number of DETs increased with developmental stage, and the largest number was observed at the awn primordium stage (W5.0), where we also observed the strongest phenotypic differentiation between the genotypes, including floral reversion and bract outgrowth in the *mnd1.a* mutant (Supplemental Fig. S12C).

We discovered a core set of DETs for all three developmental stages in the *mnd1.a* mutant that consisted of 43 transcripts (Supplemental Fig. S12C). Of the 24 upregulated core DETs, 20 showed no or very low expression levels in the inflorescence of cv Bowman and were clearly expressed in the *mnd1.a* mutant. Conversely, 12 of the 19 DETs downregulated at all stages exhibited no or very low expression levels in *mnd1.a* but were strongly expressed in the wild-type inflorescences (Fig. 6E). Genes expressed only in the inflorescence of the *mnd1.a* mutant had roles in cell cycle control, cell division, differentiation, and morphogenesis and included, for example, two ribonucleoside-diphosphate reductase large subunit genes (RNRs; HORVU2Hr1G065760.1 and HORVU3Hr1G089710.1), a RING/U-box superfamily protein (HORVU7Hr1G107430.1), two F-box superfamily proteins (HORVU1Hr1G088190.2 and HORVU6Hr1G082230.1), and two receptor kinase genes (HORVU2Hr1G037740.1 and HORVU7Hr1G115940.2; Fig. 6E; Deshaies and Joazeiro, 2009; De Smet et al., 2009; Vierstra, 2009). Moreover, transcripts with roles in light signal transduction were also primarily upregulated in the *mnd1.a* mutant and included, for example, two *FAR-RED IMPAIRED1* (*FAR1*) genes (HORVU0Hr1G038960.25 and HORVU4Hr1G014170.1; Fig. 6E), which have multiple roles in plant development, including meristem as well as floral development (Wang and Wang, 2015; Liu et al., 2016). Interestingly, transcripts of Lys-specific demethylase 5D (HORVU2Hr1G045000.1) were detected only in Bowman, and not in apices of the *mnd1.a* mutant (Fig. 6E). Functions of Lys-specific demethylases include demethylation of Lys residues on histones that regulate chromatin structure and, thereby, gene expression including that of the central floral homeotic genes (Jiang et al., 2007; Jeong et al., 2009).

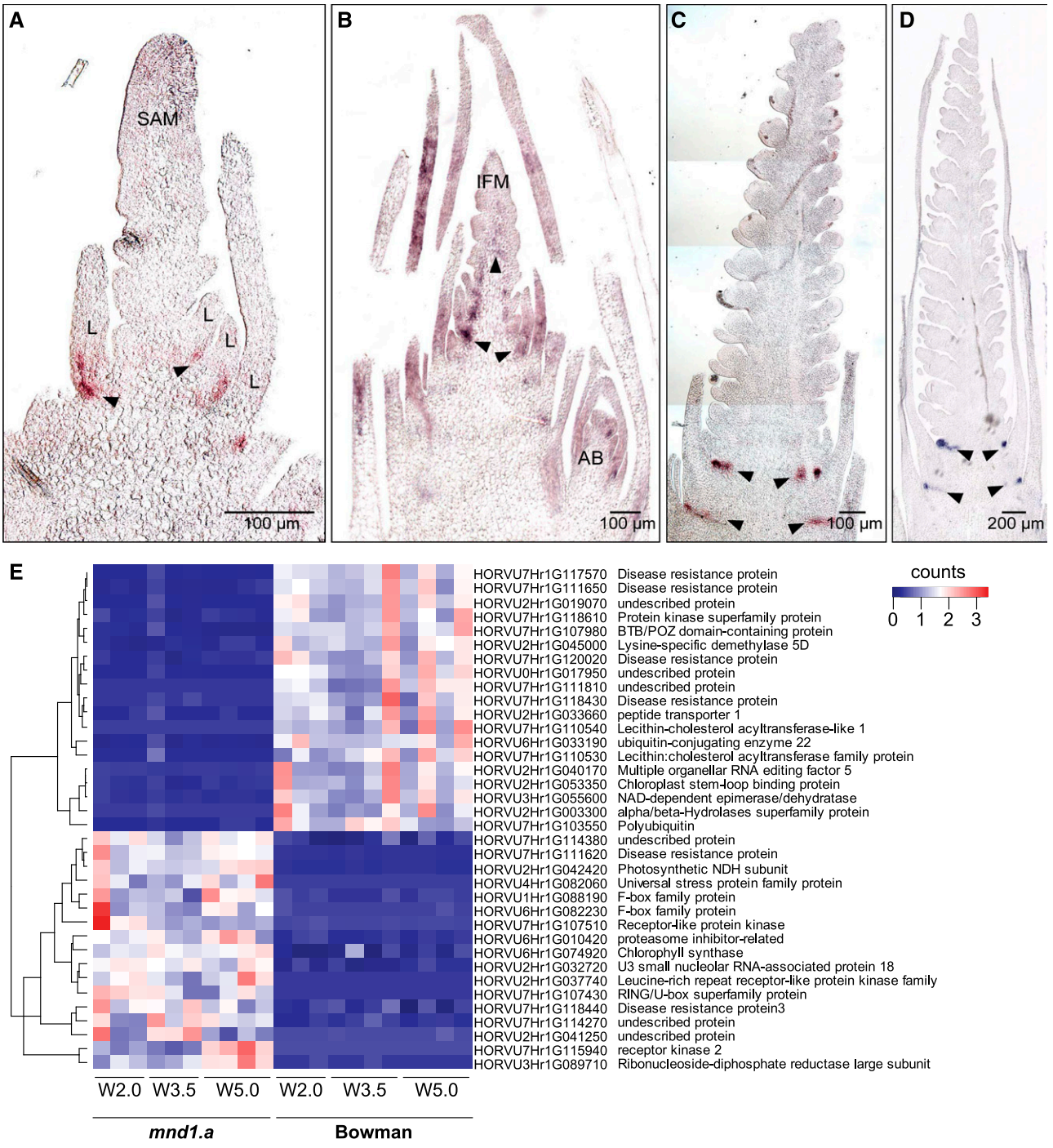

Figure 6. *HvMND1* expression and transcriptome analysis in developing inflorescences. A to D, Longitudinal sections of cv Bowman SAMs before floral transition (W1.0–W1.5; A), at the spikelet primordium initiation stage (W2.0; B), at the glume stage (W3.0, stitched and fused to assemble a single image; C), and at the awn primordium stage (W5.0; D), hybridized with an *HvMND1* antisense probe. Expression of *HvMND1* is restricted to the base at the abaxial site of developing leaves and in the inflorescence at W2.0 (marked by arrowheads). IFM, Inflorescence meristem; L, leaf. E, Heatmap of core DETs showing a significant regulation (LogFC ≤−1.5 or ≥1.5; false discovery rate ≤0.05) at all three investigated developmental stages of *mnd1.a* inflorescence (W2.0, W3.5, and W5.0). The number of raw counts for each gene in each biological replicate is color coded.

Furthermore, several transcripts involved in biotic and abiotic defense were partly or completely downregulated in *mnd1.a* inflorescences, including three putative nucleotide-binding site Leu-rich repeat resistance genes (HORVU7Hr1G111650.1, HORVU7Hr1G117570.5, and HORVU7Hr1G120020.16; Fig. 6E). These results suggest that the *mnd1.a* mutation caused changes in the tissue-specific expression of genes that have functions in cell cycle control, development, and defense across all three developmental stages.

We further investigated transcriptional changes for each developmental stage separately to identify transcripts linked to the stage-specific phenotypic differences between wild-type and mutant plants (Supplemental Dataset 2). We found an enrichment of photosynthesis-related DETs in *mnd1.a* inflorescences at the spikelet initiation stage (W2.0). For example, several genes encoding for chlorophyll *a/b*-binding proteins, which are part of the light-harvesting complex, and PSI and PSII subunits were upregulated in the *mnd1.a* mutant compared to cv Bowman. Notably, these expression changes in photosynthesis-related genes coincide with the derepression of inflorescence bract development followed by the outgrowth of bracts into leaf-like structures in the mutant. In *mnd1.a* inflorescences at the stamen primordium (W3.5) and awn primordium (W5.0) stages, we observed changed expression of several genes that are implicated in developmental control. For example, four *LIGHT-DEPENDENT SHORT HYPOCOTYLS* (*LSH*) genes (HORVU2Hr1G089190.3, HORVU3Hr1G088000.1, HORVU6Hr1G058340.3 and HORVU6Hr1G088790.1) were upregulated. Members of the LSH protein family are known suppressors of organ differentiation in boundary regions in Arabidopsis and rice (Takeda et al., 2011; Yoshida et al., 2013). Furthermore, seven barley *MADS-box* (*BM*) genes were downregulated in *mnd1.a* inflorescences at W3.5 and W5.0. *MADS-box* genes encode floral homeotic transcription factors that are involved in flower development and vegetative organogenesis (Davies and Schwarz-Sommer, 1994; Trevaskis et al., 2007). These *BM* genes included barley homologs of floral patterning genes, such as *APETALA1* (*AP1*)-like (*HvBM8*; HORVU2Hr1G063800) and a *SEPALLATA*-like gene (*SEP1*; HORVU5Hr1G095710), that were differentially regulated at the stamen primordium stage. In addition, transcripts of *LEAFY* (*LFY*; HORVU2Hr1G102590.2), which is involved in the initiation of floral meristems as well as tillering and panicle branching, were reduced in *mnd1.a* (Weigel et al., 1992, Rao et al., 2008). Moreover, we observed a strong upregulation of two *TERMINAL FLOWER1* (*TFL1*)-like genes in *mnd1.a* shoot apices (HORVU2Hr1G072750.4 and HORVU4Hr1G078770.1). *TFL1*-like genes are key repressors of flowering time and regulators of shoot architecture (Shannon and Meeks-Wagner, 1991; Bradley et al., 1996; Pnueli et al., 1998; Nakagawa et al., 2002). Among the identified *TFL1*-like DETs was the barley homolog of snapdragon (*Antirrhinum majus*) *CENTRORADIALIS* (*HvCen*), an important regulator of seasonal flowering and growth habit that has been targeted during barley improvement (Comadran et al., 2012; Bi et al., 2019). The upregulation of floral repressors (*TFL1-like* and *LSH*) and downregulation of floral inducers (*BM*) was associated with the delayed floral development in the *mnd1.a* mutant. In addition, several homeobox-Leu zipper protein family genes (*HOX*) were differentially regulated in developing *mnd1.a* inflorescences at W3.5 and W5.0. Among them, two *WUSCHEL-related HOX* (*WOX*) transcription factor genes (HORVU2Hr1G113820.5 and HORVU4Hr1G051530.8) showed higher transcript levels in the mutant. *WOX* genes confer several regulatory roles in plants, including stem cell maintenance, cell proliferation, floral transition, and lateral organ formation (Wu et al., 2007; Vandenbussche et al., 2009; Dolzblasz et al., 2016). We also observed changes in transcript levels of several genes controlling shoot and spike architecture. For example, transcript levels of four *TEOSINTE-LIKE1*, *CYCLOIDEA*, and *PROLIFERATING CELL FACTOR1* (*TCP*) transcription factor family genes were increased in *mnd1.a* inflorescences at W5.0 (HORVU7Hr1G038130.1, HORVU6Hr1G075650.1, HORVU3Hr1G073830.1, and HORVU5Hr1G000490.1), of which HORVU5Hr1G000490.1 encodes for a *TEOSINTE BRANCHED1* (*TB1*)-like *TCP* transcription factor. This gene showed expression in *mnd1.a* developing inflorescences, but transcripts were absent in cv Bowman inflorescences at W3.5 and W5.0. However, barley *TB1* (HORVU4Hr1G007040) and *GRASSY TILLERS1* (*GT1*; HORVU4Hr1G070610), which acts downstream of *TB1* to control lateral bud outgrowth (Whipple et al., 2011), were not differentially regulated in the *mnd1.a* mutant. *HvMND1* itself showed overall lower transcript levels in mutant apices than in cv Bowman at all three investigated stages.

Taken together, our transcriptome analysis revealed a core set of DETs consistently regulated at all investigated stages of inflorescence development in the *mnd1.a* mutant. A high proportion of the core DETs showed expression in mutant inflorescences, but transcripts were absent in cv Bowman, and vice versa. Most of these transcripts are associated with regulatory functions in cell cycle control and development. Furthermore, genes controlling phase-change transitions, floral meristem identity, and floral development were particularly differentially regulated during inflorescence development (W3.5 and W5.0) in *mnd1.a*. We therefore hypothesize that *HvMND1* is a regulator of organ-specific expression of genes involved in cell proliferation and meristem transitions.

The *mnd1.a* Mutant Exhibits Altered Expression Levels of the Developmental miRNAs *miR156* and *miR172*

The pleiotropic *mnd1.a* phenotype and differential regulation of floral homeotic genes were reminiscent of the effects caused by misregulation of the developmental

miRNAs *miR156* and *miR172*. The sequential expression of *miR156* and *miR172* regulates phase change and plant architecture in different plant species (Schwab et al., 2005; Xie et al., 2006; Wu et al., 2009). We therefore tested whether the *mnd1.a* phenotype was linked to changes in the levels of *miR156* and *miR172* in the developing apices of Bowman and the *mnd1.a* mutant. We collected main SAMs and surrounding leaves from mutant and wild-type plants over a time period of 1 to 32 d after emergence (DAE) and determined the Waddington stages at each sampling time point. The analysis revealed significant differences in the transcript levels of both miRNAs. When miRNA abundance was compared between the two genotypes for several days after plant emergence, *miR156* levels decreased in both lines but were significantly higher in the *mnd1.a* mutant than in cv Bowman until 18 DAE (Fig. 7A). In contrast, levels of *miR172ac* and *mR172b* increased and were significantly lower in the mutant than in the wild type between 14 and 32 DAE and between 18 and 25 DAE, respectively (Fig. 7, B and C). The delays in vegetative phase change and floral development in *mnd1.a* were therefore linked to higher levels of *miR156* and reduced levels of *miR172* in the apex. When differences in the miRNA abundance were compared between genotypes across the same stages, *miR156* levels were significantly higher in *mnd1.a* compared to cv Bowman only during the early vegetative stage (Fig. 7D). The mature *miR172ac* and *miR172b* transcripts were significantly higher in the mutant than in cv Bowman at spikelet initiation (W2.0) and the glume primordium stage (W3.0; Fig. 7, E and F). We further investigated the expression of seven *SQUAMOSA PROMOTER BINDING PROTEIN-LIKE* (*SPL*) genes in barley, which carry putative miR156 target sites (Tripathi et al., 2018). The expression of *SPL3*, *SPL11*, *SPL13*, *SPL16*, and *SPL18* showed a gradual increase in expression over time in cv Bowman (Supplemental Fig. S13). Expression of *SPL17* and *SPL23* could not be detected in our study. In the *mnd1.a* mutant, all *SPL*-like genes showed significantly lower expression, and the gradual increase in expression over time was less pronounced, as observed in cv Bowman, with the exception of *SPL16*, which did not display significant expression differences between cv Bowman and the mutant. When comparing the expression of the *SPL*-like genes between genotypes at the same developmental stages, all *SPL*-like genes, except for *SPL3*, showed increased expression in the mutant similar to the changes in *miR172* transcript abundance at the same developmental stages.

Taken together, the delay in vegetative phase transition and reproductive development in *mnd1.a* was associated with a delay in the downregulation of *miR156* and upregulation of *miR172* over time. However, comparison of *miR172* levels across genotypes at the same stage revealed that *mnd1.a* mutants exhibited significantly higher levels of *miR172* levels at the reproductive stages compared to cv Bowman.

DISCUSSION

We identified *HvMND1*, an acyl-CoA *N*-acyltransferase, as a regulator of developmental phase change in barley. *HvMND1* had pleiotropic effects on many shoot and inflorescence architecture traits. The SAM of *mnd1.a* mutant plants remained vegetative for a longer period and generated more leaves on the main shoot. Leaves in the *mnd1.a* mutant were smaller, possibly due to a

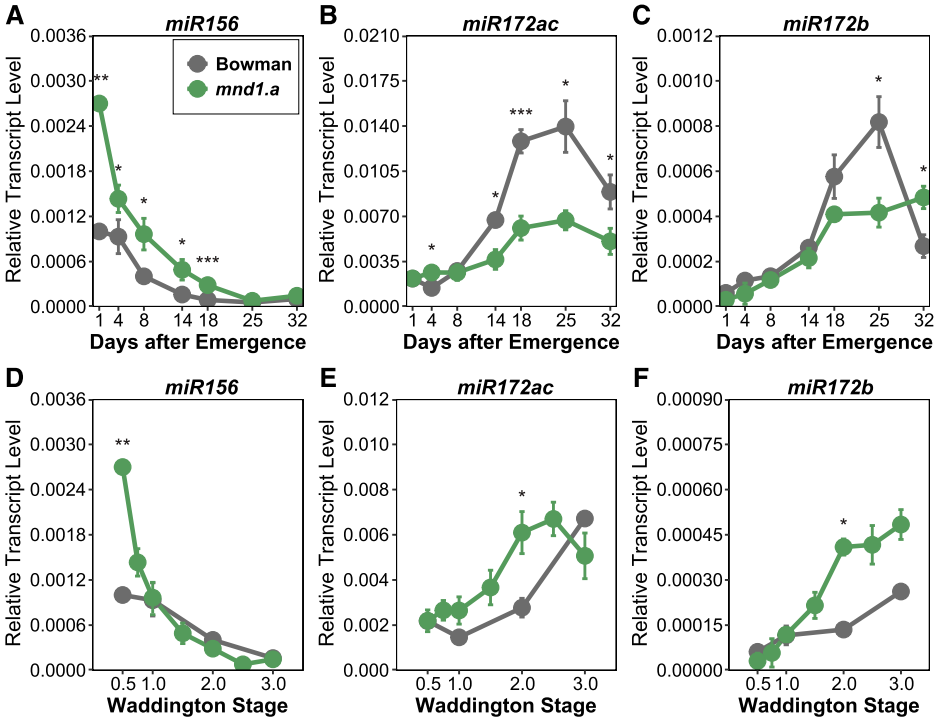

Figure 7. Transcriptional changes of the developmental miRNAs *miR156* and *miR172* in the *mnd1.a* mutant. A to C, Mature *miR156* (A), *miR172ac* (B), and *miR172b* (C) transcript levels were monitored for cv Bowman and *mnd1.a* mutant plants from 1 to 32 DAE. D to F, miRNA transcript levels of cv Bowman and *mnd1.a* samples were compared according to developmental stage (W0.5–W3.0). Values represent means ± SD ($n = 3$ biological replicates per genotype). Statistical significance was assessed by a two-tailed unpaired Student's *t* test (*$P < 0.05$, **$P < 0.01$, and ***$P < 0.001$).

shorter cell proliferation phase and faster leaf maturation linked to a shortened phyllochron, while the leaf initiation rate was not altered. The higher number of fast-outgrowing leaves was associated with an increased number of initiated ABs and tillers, suggesting that the increase in leaf number leads to the high-tillering phenotype in the *mnd1.a* mutant. As such, the *mnd1.a* phenotype resembles barley *mnd6* and rice *pla1* mutants characterized by increased leaf production and short plant stature (Itoh et al., 1998; Miyoshi et al., 2004; Mascher et al., 2014). However, *MND6* and *PLA1* encode for cytochrome p450 proteins, which are neither related to the *MND1* gene nor differentially regulated in the *mnd1.a* mutant plants. In contrast to *mnd6* and *pla1*, *mnd1.a* mutants showed a strong delay in the transition from vegetative to reproductive growth. Furthermore, not only was the transition to reproductive growth delayed in the *mnd1.a* mutant, but the successive progression of vegetative to reproductive growth was impaired. The induction of vegetative structures continued even after the transition to reproductive growth so that the mutants exhibited an overlap of vegetative and reproductive development. These were the development of tillers at aerial nodes and the derepression of bracts coinciding with the reversion of triple-spikelet meristems to vegetative branch meristems. Bracts have been proposed to act as signaling centers regulating the fate of the correlated floral meristems (Whipple, 2017). Insufficient bract suppression might therefore have affected the determinate fate of triple-spikelet meristems and subsequent reversion to branch meristem-like organs in the *mnd1.a* inflorescences.

Floral reversion, bract development, and AB growth at aerial nodes in the *mnd1.a* mutant indicated reduced apical dominance (Cline, 1997; Cline, 2000). Apical dominance is established by the phytohormone auxin that is produced in the growing shoot tip and transported downward to suppress bud outgrowth (Müller and Leyser, 2011; Gallavotti, 2013). Reduced apical dominance in the *mnd1.a* mutants therefore indicated reduced auxin production or transport. The release of bract outgrowth, spikelet meristem reversion, and reduced lateral spikelet development in the *mnd1.a* mutant were only observed at basal inflorescence nodes, and these phenotypes gradually diminished toward the apical inflorescence. Basal-distal gradients in spike morphology have been observed before and are associated with gradients in gene expression (Debernardi et al., 2017) and in cytokinin, gibberellin, and auxin levels along the spike (Youssef et al., 2017), suggesting that the *mnd1.a* mutation interacted with gene expression or hormone level differences across the inflorescence. In addition, the outgrowth of branches at aerial nodes subtending the inflorescence, as well as the floral reversion and strong vegetative program of the *mnd1.a* mutant, indicated reduced apical dominance. Interestingly, the *mnd1.a* mutant plants continued to generate tillers much longer than those of wild-type plants, suggesting that *HvMND1* controls longevity and whole-plant senescence in barley. These profound changes in the developmental program resulted in mutant plants with increased vegetative and decreased reproductive biomass. Similar phenotypes have been described for the maize mutant *Corngrass1* (*Cg1*) which is characterized by overproduction of leaves and inflorescences with changed floral architecture and abolished bract suppression (Poethig, 1988; Chuck et al., 2007). Similarly, the rice mutant *pla1* develops ectopic shoots at primary rachis branches that are subtended by outgrown and enlarged bracts (Miyoshi et al., 2004). These aberrations in the timing of reproductive and vegetative transitions, including changes in the strict temporal and spatial progression of developmental events, have been termed heterochrony. In plants, heterochronic changes have been identified in gametophyte development, embryogenesis, vegetative development, shoot maturation, and floral morphogenesis and were presumably responsible for many morphological innovations during land plant evolution (Li and Johnston, 2000; Buendía-Monreal and Gillmor, 2018; Pabón-Mora et al., 2019). The collective phenotypes of the *mnd1.a* mutant resemble that of a heterochronic mutant. We therefore propose that *HvMND1* is a heterochronic gene that controls phase change in barley.

We demonstrated that *HvMND1* codes for an acyl-CoA *N*-acyltransferase. Acyltransferases are widespread among plants, yeasts, and other organisms and show a range of targets for amino group acetylation. These targets include small molecules such as auxin-related metabolites (Epstein and Ludwig-Müller, 1993), N termini of larger proteins that are blocked from degradation when acetylated (Driessen et al., 1985), and the Lys residues of histones. The latter are posttranslational modifications of histone tails that result in either permissive or repressive chromatin states modulating gene expression (Chen and Tian, 2007). Our phylogenetic analysis demonstrated that *HvMND1* has three homologs in Arabidopsis, one of which is the functionally characterized *HLS1* gene. *HLS1* is a major regulator of seedling growth that integrates environmental and endogenous hormonal signals to control the formation of the apical hook (Lehman et al., 1996). The molecular function of *HLS1* was recently demonstrated, revealing its interaction with the Mediator complex in histone acetylation (Liao et al., 2016). Similarly, the closest *HvMND1* homolog in rice (*OsglHAT1*) acetylates histone H4, and associated proteins specify its Lys acetylation spectrum (Song et al., 2015). In our protein localization experiment, we detected HvMND1 proteins not only colocalizing with the plasma membrane but also in nuclei, and we thus propose that HvMND1 might act as a regulator of gene expression through the acetylation of histones in the chromatin of specific target genes. However, we did not detect differences in the Lys acetylation of proteins in young inflorescences, probably because *HvMND1* is only expressed in a subset of cells in the SAM or might acetylate very specific proteins or target promotor sequences, as has been

observed for its rice and Arabidopsis homologs (Song et al., 2015; Liao et al., 2016). Furthermore, the spatial and temporal expression profile of *OsglHAT1* is similar to that of *HvMND1* (Song et al., 2015). In both barley and rice, expression was detected on the abaxial side of young developing leaves and only at the onset of reproductive development in developing inflorescences. Additionally, *OsglHAT1* was expressed in bracts but only during the primary and secondary branch differentiation stages of inflorescence development, suggesting a potential function in bract outgrowth repression. Transgenic knockdown *OsglHAT1* plants, like the *mnd1.a* mutants, are stunted and have smaller grains (Song et al., 2015). However, the authors do not report higher leaf and tiller numbers, bract outgrowth, or a flowering time phenotype. Our data suggest that *HvMND1* and its paralog HORVU5Hr1G071620 arose from a recent duplication event in barley, so the regulation of inflorescence development and vegetative growth by HvMND1 may be due to subsequent neofunctionalization. We did not detect expression of HORVU5Hr1G071620 in our RNA sequencing data, whereas *HvMND1* expression was clearly detected (Supplemental Dataset 2). Diversity analyses using a panel of wild and cultivated barley revealed two major haplotypes and only a few genotypes with nonsynonymous nucleotide substitutions. This strong sequence conservation indicates a functionally important protein that acts as a hub regulator of phase change and meristem development of different shoot meristems in barley.

Homology to OsglHAT1 and HLS1 suggested that HvMND1 might control gene expression through histone modifications. Indeed, the mutation in *mnd1.a* caused differential expression of 43 genes that were exclusively expressed in either the wild-type or mutant inflorescences. These transcripts showed enrichment in cell cycle-associated transcripts that were specifically expressed in the *mnd1.a* inflorescences but not in cv Bowman. Previous studies have highlighted the role of the cell cycle machinery in shaping plant architecture (Xu et al., 2012; Yang et al., 2018). It is well known that histone acetyltransferases play a crucial role in controlling cell fate and influence cell cycle progression through either histone modification of promoter regions or direct deacetylation of target nonhistone proteins or both (Telles and Seto, 2012). Consequently, HvMND1 might directly control cell cycle and proliferation. However, the enrichment in cell cycle genes might also be a consequence of the highly proliferating and morphologically different SAM and inflorescence tissue in *mnd1.a* compared to cv Bowman. Moreover, an ortholog of the Lys-specific demethylase 5D RELATIVE OF EARLY FLOWERING 6 (REF6) was not expressed in *mnd1.a* inflorescences but was present at all stages in cv Bowman. In Arabidopsis, REF6 is a histone demethylase and promotes flowering through transcriptional regulation of floral integrators such as *FLOWERING LOCUS T* (*FT*) and *SUPPRESSOR OF CONSTANS OVEREXPRESSION1* (*SOC1*; Noh et al., 2004; Lu et al., 2011). Such methylation marks located at histones, including marks at Lys residues, maintain repression of their target genes and are important for correct expression of plant developmental genes (Zhang et al., 2007). Consequently, HvMND1 likely acts as an epigenetic modifier to turn on or off the expression of a core set of genes that are putatively involved in regulating meristem identity and development. In addition, *mnd1.a* was characterized by altered expression levels of the sequentially expressed miRNAs *miR156* and *miRNA172*. Typically, the sequential transcript levels of *miR156* and *mR172* are negatively correlated. The *mnd1.a* mutant, however, displayed high levels of both *miR156* in the early vegetative phase and *miR172* in the reproductive inflorescence. Overexpression of *miR156* in the dominant *Cg1* mutant in maize caused a delay in juvenile-to-adult phase change, an increase in the number of leaves and tillers, a delay in flowering, and development of small ears with large bracts (Chuck et al., 2007). Similarly, a semidominant rice mutant, *Bushy dwarf tiller1* (*Bdt1*), with increased expression of *miR156*, displayed high tillering and small panicles with overgrown bracts and leaf-like structures (Hayashi-Tsugane et al., 2015). In addition, overexpression of *miR172b* in rice delayed the transition from spikelet meristem to floral meristem. This resulted in defects in floral and grain development, including changes in the number and identity of floral organs and reduced fertility and grain weight (Zhu et al., 2009). miRNAs bind to complementary sequences within mRNA molecules and cause silencing of these mRNA molecules by cleavage, destabilization, or reduced protein translation (Bartel, 2009). *miR156* targets the *SPL* gene family encoding plant-specific transcription factors that control leaf, floral, and fruit development in different plants (Rhoades et al., 2002; Bonnet et al., 2004; Xie et al., 2006; Tripathi et al., 2018). In *mnd1.a*, high expression levels of *miR156* in the early vegetative phase were associated with a reduction in *miR156*-targeted *SPL* transcript levels, such as those of *HvSPL3* and *HvSPL13*. In rice, increased expression levels of *miR156f* in the *Oryza sativa multi-tillering and dwarf1* (*osmtd1*) mutant reduced the transcript levels of its targets *OsSPL3*, *OsSPL12*, and *OsSPL14*, resulting in a pleiotropically changed shoot architecture characterized by high tillering, aerial tillering, dwarfism, and reduced grain yield (Liu et al., 2015). Furthermore, the rice homolog OsSPL13, a target of *miR156* in rice, controls grain size by altering grain thickness and length, as well as panicle length and branch number (Si et al., 2016). Consequently, altered expression levels of these miRNAs and *miR156*-targeted *SPL* genes may have caused some of the pleiotropic phenotypes in the *mnd1.a* mutant. Histone acetylation by epigenetic modifiers is associated with the gradual downregulation of *miR156* in Arabidopsis (Kim et al., 2015; Picó et al., 2015; Li et al., 2017; Xu et al., 2018). *HvMND1* may therefore act as a positive regulator of the vegetative-to-reproductive phase transition by epigenetic control of *miRNA156* and/or *miRNA172* expression.

However, further biochemical studies of acetylation targets of HvMND1 should be conducted to determine its molecular function.

The delay in spikelet initiation observed for the *mnd.1a* mutant was associated with the downregulation of the floral homeotic *LFY* gene and the upregulation of floral repressor *TERMINAL FLOWER1* (*TFL1*/*CEN*) at the stamen primordium stage. *LFY* and *TFL1* act antagonistically in the meristem for the acquisition of a floral meristem fate in Arabidopsis and rice, and changes in the dosage of either of these genes have strong effects on timing of the reproductive phase transition (Ratcliffe et al., 1998; Rao et al., 2008; Nakagawa et al., 2002). We also observed the downregulation of MADS-box transcription factors involved in floral development and patterning, such as barley homologs of *PI*, *SEPALLATA*, and *AP1*/*FUL*. Interestingly, rice double mutants for the *AP1*/*FUL*-like genes *OsMADS14* and *OsMADS15* exhibited AB formation at stem nodes, delayed flowering, derepression of bracts, and floral reversion in the inflorescence comparable to the inflorescence phenotypes we observed for the *mnd1.a* mutant (Kobayashi et al., 2012; Wu et al., 2017). Similarly, inflorescences of Arabidopsis *soc1-3 ful-2* double mutants show floral reversion, the generation of many small leaves with AXMs, and bract formation (Melzer et al., 2008). In addition, the mutant plants were characterized by secondary growth and survival of stems and apical rosettes, while the wild-type plants senesced and died after seed maturation. We also observed a significant increase in the longevity and ability to generate new tillers even after the transition to flowering in the *mnd1.a* mutant, while cv Bowman plants underwent whole-plant senescence after flowering. Furthermore, the *SHORT VEGETATIVE PHASE* (*SVP*)-like gene *BM1* was upregulated in the *mnd1.a* apices. Overexpression of *BM1* causes reversion of spikelet meristems to branch meristems at the inflorescence base and late flowering due to an extended reproductive phase in barley (Trevaskis et al., 2007). In rice, the *tawawa1-D* (*taw1*) mutant, carrying a gain-of-function mutation in an Arabidopsis LSH1 and *Oryza* G1 (ALOG) family protein, also showed increased inflorescence branching. Lateral meristems acquired a branch-meristem rather than a spikelet-meristem identity through upregulation of the SVP family genes *OsMADS22*, *OsMADS47*, and *OsMADS55* (Yoshida et al., 2013). Similarly, the upregulation of LSH-encoding transcripts and SVP-like genes in the *mnd1.a* mutant was linked to the formation of branch meristems instead of spikelet meristems at the base of the inflorescences. Consequently, reversion of spikelet meristems to branch meristems and longevity in *mnd1.a* were likely the consequence of changes in the expression dosage of floral homeotic genes.

The phenotype of the *mnd1.a* mutant is interesting also from an evolutionary perspective. It shares several features with the wild progenitor of barley and *Hordeum* sp. from the secondary and tertiary gene pool, such as a more pronounced vegetative program, prolonged tillering, and a reduced ratio of reproductive to vegetative biomass (Kernich et al., 1995). Selection and breeding of modern barley may have caused a progressive reduction in the vegetative program or the relative duration of the juvenile and adult phases of shoot development. Since spike size is generally related to the duration of the reproductive phase, human selection for large spikes may have resulted in the suppression of juvenile traits. However, sequencing of *HvMND1* in diverse accessions did not reveal strong differences between cultivated and wild barley. Future studies need to analyze differences between the expression domains or levels of *HvMND1* and relevant target genes in wild and cultivated barley.

Taken together, we propose that HvMND1, identified as an acyl-CoA *N*-acyltransferase, is a positive regulator of the vegetative-to-reproductive phase change, possibly by coordinating expression of the genes involved in phase transitions and floral development in barley.

MATERIALS AND METHODS

Plant Material and Cultivation

Barley (*Hordeum vulgare*) seeds of the original *mnd1.a* mutant line in the background of cv Mesa, the derived backcross line in the background of cv Bowman, as well as the parental cultivars Bowman and Mesa, were obtained from the U.S. Department of Agriculture (Supplemental Table S7). Seeds of the *mbd* mutant, the parental cv ZOH, MHOR198, and HOR3069 were obtained from the Leibniz Institute of Plant Genetics and Crop Plant Research. Previously identified mutations of both mutant lines are summarized in Supplemental Table S7.

Outdoor Plant Cultivation and Phenotyping

The original and backcrossed *mnd1.a* mutant, as well as the respective parental cultivars, were sown in 96-well trays in February of 2014 and 2015. Plants germinated in the greenhouse and were transferred to 12-L pots with one plant per pot and at least 16 replicates per genotype. The soil was composed of peat and a clay-soil mixture (Einheitserde, Einheitserdewerke Werkverband) and was supplemented with long-term fertilizer. Plants were cultivated outdoors in Cologne, Germany, irrigated with a sprinkling robot, and fertilized or treated with pesticides, as described previously (Liller et al., 2015). The pots were randomized and arranged in 22 rows, with 54 pots per row placed at a distance of 10 cm. The plots were surrounded by one row of pots with cv Morex plants to ensure an even planting density for every experimental plant. At 89 DAE, plant pictures were taken of one representative plant per genotype. Flowering time was measured in days from plant emergence until the appearance of the first awns from the flag leaf, called tipping. At plant maturity, ~2 weeks before harvest, tiller numbers were counted at the base of each plant and plant height was measured (from soil surface to the base of the uppermost spike). After harvest in the year 2015, whole plants were dried for 2 weeks, spikes were removed, and the vegetative dry weight of each plant was determined. Exemplary spikes for each genotype were scanned. Grain measurements were performed on three to five spikes of one plant, and five plants per genotype, of the 2014 and 2015 outdoor trial. Grain cleaning was performed by hand for each spike individually and measurements were performed using the MARVIN Seed Analyzer (GTA Sensorik) to assess the number of grains per spike, the TGW, and grain length, width, and area.

Greenhouse Cultivation and Phenotyping

For detailed macroscopic phenotyping of the investigated *mnd1.a* mutant, cv Bowman and the *mnd1.a* NIL were sown in 96-well trays (Einheitserde, Einheitserdewerke Werkverband). After stratification for 3 d at 4°C, plants were

cultivated in controlled LD greenhouse chambers (Bronson Climate) with 16 h light (22°C; photosynthetic photon flux density [PPFD] 270 μm m^{-2} s^{-1})/8 h dark (18°C) day/night cycles. After emergence of the second leaf, plants were transferred to 20-well growing trays. At 3 DAE and subsequently every week after emergence, five plants per genotype were dissected until the end of the experiment at 9 WAE. At each time point, the developmental stage of the SAM of the main stem was determined according to the quantitative scale introduced by Waddington et al. (1983) using the stereomicroscope Nikon SMZ18 and NIS-Elements BR software (version 3.4; Nikon Instruments Europe). In addition, the number of visible leaves, tillers, and elongated internodes (distance to previous node >5 mm) were counted at each time point. To study phyllochron in wild-type cv Bowman and *mnd1.a* mutant plants, leaf emergence rates during the first 5 WAE were compared. Phyllochron was calculated as the leaf emergence $rate^{-1}$ from the slope of the linear regressions in R (R version 3.3.2; R Development Core Team, 2011). We used the tidy function of the "broom" package (Robinson and Hayes, 2018) to extract the significance of the fitted linear regression, the slope (phyllochron), and the SE. The number of spikelet primordia was counted for main shoot apices from the stage of pistil primordium initiation (W4.0) until the stage of style formation (W6.0), and length of the main inflorescences was measured for each plant from spikelet initiation (W2.0) until style formation (W6.0). For the first three developed leaves, leaf length and width and the corresponding sheath length were determined when leaves were mature. At 1, 3, and 5 WAE, the number of initiated leaves was counted for five representative plants per genotype. At the same time, each leaf axil was examined for the presence or absence of an AB or tiller. ABs were classified into young ABs (AXM surrounded by only one leaf) or mature ABs (AXM enveloped in more than one leaf and potentially with secondary ABs formed). As bud outgrowth progressed, we further classified tillers into young tillers with only one shoot visible or mature tillers with secondary side shoots apparent. At 1, 3, and 5 d after germination, the length of the first leaf was measured to investigate the rate of leaf elongation for each genotype. To study the wild-type and *mnd1.a* plastochron, the number of all initiated leaves, including leaf primordia, was counted for seedlings 1 to 5 d after germination in daily intervals. The plastochron was calculated as the leaf initiation $rate^{-1}$, analogous to calculation of the phyllochron. In a separate experiment, *mnd1.a* NILs in cv Bowman and the original *mnd1.a* mutant line, as well as the corresponding parental lines, were germinated in 96-well trays, and single plants were repotted to 1-L pots when the two-leaf stage was reached to investigate the duration of tiller development. The plants were grown in greenhouses under LD conditions as described above. Watering, application of fertilizer, and pesticide treatments were conducted regularly and continued even a few weeks after plants senesced to monitor new leaf and tiller outgrowth. Additionally, completely dried, ripe spikes were cut to prevent new tiller outgrowth from accidently dispersed grains without pruning the plant. New outgrowth was recorded visually and images of plants were taken 3, 4, and 5 months after plant emergence. The experiment was terminated after 12 months.

Cell Size Measurements in the Leaf Epidermis

Cell size measurements were conducted on five mature L1 leaves per genotype of plants at 3 WAE grown under controlled LD conditions as described above. The length of the leaf blade was determined. A 2-cm interval marked at 33% and 66% of the leaf blade length was thinly brushed with 5% (w/v) cellulose acetate dissolved in acetone. After drying, epidermal imprints were carefully removed with tape and attached to microscope slides. The length of five cells at 33% and 66% of the leaf blade length of each plant was measured for each of the following cell types: blade lateral cell, blade cell between veins, blade cell between veins and next to lateral cells, over vein cell, over vein cell and next to sclerenchyma cells, over vein cell and next to lateral cells, and cells in the stomatal row (see Wenzel et al. [1997] for cell type terminology). A Nikon SMZ18 stereo microscope with the NIS-Elements BR software (version 3.4; Nikon Instruments Europe) was utilized for cell measurements.

Scanning Electron Microscopy

Dissected main inflorescences were mounted on a copper specimen holder with freeze-hardening glue and fast-frozen in liquid nitrogen. Using a transfer unit, meristems were moved to an airtight cryo chamber (K1250X, Emitech). After sublimation, meristems were chilled and subsequently coated in palladium and gold for imaging. Meristem morphology was observed using a Zeiss Supra 40VP scanning electron microscope. Images were processed with Adobe Photoshop to remove the background of the electron micrographs.

RNA Sample Preparation and RNA Sequencing

Inflorescences of main culms from cv Bowman, cv Mesa, and the backcross-derived *mnd1.a* mutant grown in controlled LD greenhouse chambers (Bronson Climate) with 16 h light (22°C, PPFD 270 μm m^{-2} s^{-1})/8 h dark (18°C) day/night cycles were used for RNA isolation. The following stages of inflorescence development were selected: spikelet initiation (W2.0), stamen primordium stage (W3.5), and awn primordium (W5.0). In the case of cv Mesa plants, only vegetative SAM tissue (W1.0) was harvested. Collected tissues included the SAM, its base, and small surrounding leaves and were sampled in the middle of the day, 6 to 7 h before the onset of the night period (Supplemental Fig. S14). To assure that all samples were collected at the correct stages, three plants per genotype were dissected before sampling. At least three separate biological replicates, each consisting of a pool of at least 10 meristems, were collected. RNA sample preparation, RNA sequencing, quality control, and adaptor trimming were performed as described in van Esse et al. (2017). Additionally, vegetative SAMs (W1.0–W1.5) from cv Mesa plants grown at the same conditions were harvested and total RNA was extracted. Two biological replicates of cv Mesa SAMs with at least 10 pooled meristems were subjected to RNA sequencing.

Single-Nucleotide Polymorphism Calling and Candidate Gene Selection

Reads obtained from sequencing the total mRNA of SAMs were mapped to a combined set of high-confidence and low-confidence CDSs of the recently described genome of barley 'Morex' (Mascher et al., 2017). For single-nucleotide polymorphism detection, all reads obtained from one genotype were pooled regardless of developmental stage to enable better coverage of expressed transcripts and ultimately more support for called variants. The alignments to the reference CDSs were performed using BWA-MEM (version 0.7.15; Li, 2013). Mapped reads were filtered and processed as described in van Esse et al. (2017). Subsequent variant calling was performed using the UnifiedGenotyper of GATK (version 3.6; McKenna et al., 2010). Although barley is a diploid plant species, we treated the reads as originating from a haploid species to preclude heterozygous calls and adjust the variant calling to inbreeding plant features. In addition, a minimum Phred-scaled confidence threshold for calling and emitting of single-nucleotide polymorphisms was set to 30.0 and 10.0, respectively. Variants were filtered in a custom R script (R version 3.3.2; R Development Core Team, 2011) that only allowed for variants with support of at least 30 in read depth, at least 98 for genotype quality, and a Phred quality score of >2,000. Introgression regions were defined by comparing filtered variants of *mnd1.a* and cv Bowman. Candidate genes were selected when a variant observed for *mnd1.a* was not detected in either cv Bowman, cv Mesa, or the reference of cv Morex. Pairwise alignments of translated candidate protein sequences were performed using MUSCLE (Edgar, 2004) to reveal nonsynonymous variants. Location of conserved domains were assigned using the National Center for Biotechnology Information Conserved Domain Database (Marchler-Bauer et al., 2015). Further, candidate variants were evaluated by PROVEAN (for Protein Variation Effect Analyzer; http://provean.jcvi.org), a software that computationally predicts the influence of single amino acid substitutions on protein biological function. The pairwise sequence alignment-based score (PROVEAN score) measures the change in sequence similarity of a query sequence to a protein sequence homolog before and after introducing an amino acid variation to the query sequence (Choi and Chan, 2015). The mutations in the chosen candidate genes were confirmed by Sanger sequencing using the primers listed in Supplemental Table S8.

Complementation Tests

Allelism tests were performed through crosses between the backcross-derived *mnd1.a* mutant line in cv Bowman and the shoot architecture mutants *mbd* and MHOR198 in the cv ZOH and cv HOR3069 background, respectively. Plants used for crosses were grown in LD greenhouses, emasculated, and pollinated with pollen from a single plant. Backcross-derived *mnd1.a* mutants were used as pollen donors in this study. The F1 progeny of the two crossing combinations *mbd* × *mnd1.a* and MHOR198 × *mnd1.a* was genotyped using Sanger sequencing spanning the *mnd1.a*-specific 8-bp insertion in candidate gene HORVU7Hr1G113480.3 with the primers listed in Supplemental Table S8. True heterozygous crosses were grown in greenhouse LD conditions along with the parental mutant lines and the respective genetic background parents. Parental lines and F1 progeny of MHOR198 × *mnd1.a* crosses were

vernalized for 8 weeks at 4°C in a plant growth chamber. Flowering time was assessed in days after emergence until tipping; height, tiller number, node number, and aerial branching were assessed when plants senesced. Plant pictures were taken when most of the analyzed genotypes were flowering.

Phylogenetic Analysis

To identify homologs of *HvMND1*, a BLASTP search was performed using the HvMND1 protein sequence as query against peptide sequences from the following species: *Aegilops tauschii*, Arabidopsis (*Arabidopsis thaliana*), *Brachypodium distachyon*, papaya (*Carica papaya*), cucumber (*Cucumis sativus*), barley, *Medicago truncatula*, rice (*Oryza sativa*), poplar (*Populus trichocarpa*), common bean (*Phaseolus vulgaris*), castor bean (*Ricinus communis*), sorghum (*Sorghum bicolor*), rye (*Secale cereal*), foxtail millet (*Setaria italica*), tomato (*Solanum lycopersicum*), *Selaginella moellendorffii*, wheat (*Triticum aestivum*), grapevine (*Vitis vinifera*), and maize (*Zea mays*). For barley, the current database of predicted peptide sequences was used (Mascher et al., 2017). For all other species the Phytozome 12.1.6 database (Goodstein et al., 2012) was used to retrieve homologous proteins. BLAST results were filtered with an E-value cutoff of 1E−10. The nucleotide CDSs of the homologous proteins were then extracted, one representative isoform was selected in case of alternative splicing variants, and sequences were aligned using MUSCLE (Edgar, 2004) in MEGA version 5 (Tamura et al., 2011) based on translated codons. Visually unaligned leading or trailing nucleotide sequences were removed manually from the multiple sequence alignment. The conversion to phylip format was performed using a stream editor (sed) script. The maximum-likelihood tree was generated using RAxML 8.2.10 (fixed-base frequencies, GAMMA model, and "autoMRE" for an optimal number of bootstrap repeats; Stamatakis et al., 2008). Dendroscope 3 (Huson and Scornavacca, 2012) was used for visualization of the tree, which was rooted using *S. moellendorffii* as the outgroup.

Diversity Analysis of *HvMND1*

A haplotype analysis of *HvMND1* was performed based on exome resequencing data from 39 research/breeding lines, 137 landraces, and 91 wild barley accessions published in Russell et al. (2016). Polymorphisms of the CDS of *HvMND1*, which is located on morex_contig_1619442 and morex_contig_362150, were extracted and further used to create alternate fasta sequences for each accession using a custom R script. Sequences of cv Mesa and the *mnd1.a* allele, obtained from Sanger sequencing, were added manually. A multiple sequence alignment was genereated in MEGA version 5 (Tamura et al., 2011) using the ClustalW algorithm. The median-joining network was constructed using PopART (Leigh and Bryant, 2015) with default parameters ($\varepsilon = 0$).

Analysis of DETs in the Transcriptomic Data Set of Developing Inflorescences

Whole transcriptome expression analysis was performed on the RNA sequencing reads obtained from main SAM tissues, including the base and small surrounding leaves, of cv Bowman and *mnd1.a*. The reads were aligned to the barley high-confidence transcript sequences (Mascher et al., 2017) using the quasi-mapping based mode in Salmon with default settings (Patro et al., 2015). Further processing and read quantification were performed as described in van Esse et al. (2017). DETs in *mnd1.a* mutants were selected based on adjusted $P \leq 0.05$ and log2 fold change ≤ -1.5 or ≥ 1.5. Hierarchical clustering of DETs was performed using Pearson correlation coefficients in R. The number of DETs per stage was visualized using the R package "eulerr", which generates area-proportional Euler diagrams. Gene ontology (GO) overrepresentation analysis was performed using Blast2GO (version 5.0; Götz et al., 2008) with the Fisher's exact test for significantly enriched GO terms ($P \leq 0.05$). The GO terms obtained were reduced to the most specific terms with the implemented function in Blast2GO.

RNA In Situ Hybridization and Localization in *Nicotiana benthamiana* Leaves

RNA in situ hybridizations were performed on SAMs at stages W1.0 to W1.5, W2.0, W3.5, and W5.0 as described in Kirschner et al. (2017). Plant cultivation and sampling time were according to the above-described RNA sequencing experiment ("RNA Sample Preparation and RNA Sequencing" section), although more leaves and plant base remained on the collected SAM samples. Probes for detecting the *HvMND1* mRNA were prepared from genomic DNA of barley cv Morex from the *HvMND1* start to stop codon (1,690 bp), or 861 bp upstream of the stop codon (Exon3). The DNA was cloned into the pGGC000 entry vector of the GreenGate cloning system (Lampropoulos et al., 2013) and then amplified, including the T7 and SP6 promoter sites, by PCR. RNA probes were built as described in Hejátko et al. (2006). The long RNA probes (1,609 bp) were hydrolyzed by adding 50 μL carbonate buffer (0.08 M NaHCO3 and 0.12 M Na2CO3) to 50 μL RNA probe and incubating at 60°C for 54 min. On ice, 10 μL 10% (v/v) acetic acid, 12 μL sodium acetate, and 312 μL ethanol were added, and the RNA was precipitated and dissolved in RNase-free distilled water. Polyvinyl alcohol was added to the nitroblue tetrazolium/5-bromo-4-chloro-3-indolyl phosphate staining buffer to a final concentration of 10%. Permanent specimens were created by washing the slides in 50% ethanol, 70% ethanol, 95% ethanol, and 100% ethanol for 2 min each, and in xylol for 10 s, and, after drying, adding a few drops of Entellan (Merck) and a coverslip. The construction of estradiol-inducible expression vectors with GFP as translational fusions at the C terminus for transient expression in *N. benthamiana* leaves and the transformation of *N. benthamiana* leaves was described before (Bleckmann et al., 2010). The open reading frame sequence of *HvMND1* (from genomic DNA) was inserted upstream of the fluorophore, without the stop codon and in frame with GFP. Nuclei were stained with 4′,6-diamino-phenylindole (1 μg mL^{-1}), and plasma membranes were stained with FM1-43FX (20 μM; Thermo Scientific). Pictures of the RNA in situ hybridization samples were taken using a planneofluar 10× objective with a NA of 0.30 using the Zeiss Axioskop light microscope, and image processing, i.e. stitching, was performed with the Stitching Plugin in Fiji (Preibisch et al., 2009; Schindelin et al., 2012). For imaging of the *N. benthamiana* leaves, the confocal laser scanning microscope Zeiss LSM780 with a C-Apochromat 40×/1.20 W Korr M27 was used. GFP was excited at 488 nm and emission was detected at 490 to 508 nm, 4′,6-diamino-phenylindole was excited at 405 nm and detected at 410 to 483 nm, and FM1-43FX was excited at 488 nm and detected at 545 to 668 nm.

Immunoblot Analysis of Lys-Acetylated Proteins in Inflorescence Extracts

Frozen young inflorescences in the stamen primordium stage (W3.5) were ground to a fine powder, and proteins were extracted with hot extraction buffer (0.1 M Tris-HCl [pH 7.6], 4% [w/v] SDS, and 0.1 M dithiothreitol) for 5 min at 95°C. DNA was sheared by sonication and cell debris was removed by centrifugation twice for 30 min at 18,000*g*. The supernatant was collected, and the protein yield was determined via the Pierce 660 nm Protein Assay Reagent and the compatible Ionic Detergent Compatibility Reagent (Thermo Fisher). For immunoblot analysis, 50 μg protein was separated on a 15% SDS-PAGE and transferred onto a nitrocellulose membrane. Immunodetection of Lys-acetylated proteins was performed as described previously (Hartl et al., 2015). A secondary anti-rabbit antibody IRDye 800CW was used, and infrared fluorescence signals were detected with an Odyssey FC Imaging System (Li-Cor). The membrane was afterward stained with 0.1% (w/v) amido black in 10% (v/v) acetic acid for detection of total proteins blotted.

Expression Analysis Using RT-qPCR

To study the expression of *HvMND1* in different plant tissues in cv Bowman, as well as in developing meristems of cv ZOH, RT-qPCR was performed. Wild-type cv Bowman plants were germinated on Whatman cellulose filter paper (Sigma-Aldrich) in petri dishes sealed with parafilm. Enriched seedling crown tissue containing vegetative SAMs surrounded by leaves and whole roots was sampled 3 d after germination. Plants for leaf and node tissues of cv Bowman were grown in 96-well trays, and SAM development was staged every 3 d. At W3.5, leaf material was collected from the youngest fully elongated leaves. Additionally, nodes from the uppermost elongated internode located close to the SAM were harvested. For expression analysis of *HvMND1* in cv ZOH, plants were grown in 96-well trays, and leaf-enriched developing inflorescences were collected at W1.0, W2.0, W3.5, and W5.0 as described for the RNA sequencing experiment. To determine expression of miRNAs and putative downstream targets, cv Bowman and *mnd1.a* plants were grown in 96-well trays and stem segments containing the developing SAM were sampled 1, 4, 8, 14, 18, 25, and 32 DAE. All plants were grown in chambers with 16 h light (22°C, PPFD 270 μm m^{-2} s^{-1})/8 h dark (18°C) day/night cycles, and samples were taken 6 to 7 h before onset of the night period. Three biological

replicates per tissue and genotype were collected, each consisting of a pool from three or more individual plants. Isolation of total RNA, cDNA synthesis, and RT-qPCR were performed as described in Campoli et al. (2012). RNA isolation, reverse transcription with stem-loop primers, and miRNA quantification were performed as described in Bergonzi et al. (2013). For each sample, two technical replicates were used and quantification was based on the titration curve using LightCycler 480 software (version 1.5, Roche). Transcript levels of miRNAs were normalized using Hv18S and HvsnoR23 as controls, whereas *HvMND1* and *SPL* expression levels were normalized using *HvACTIN* and *HvGAPDH*. All primers used in the RT-qPCR analysis are listed in Supplemental Table S8.

Accession Numbers

Accession numbers of all major genes and proteins mentioned in this study are listed in Supplemental Table S8. Short read Illumina data and raw variant and expression data are accessible through Gene Expression Omnibus series accession number GSE149110 (https://www.ncbi.nlm.nih.gov/geo/query/acc.cgi?acc= GSE149110).

Supplemental Data

The following supplemental materials are available.

Supplemental Figure S1. Spike and seed shape parameters of *mnd1.a* mutants in cv Bowman and cv Mesa.

Supplemental Figure S2. Internode and detailed leaf phenotype of the *mnd1.a* mutant.

Supplemental Figure S3. Impaired inflorescence development in *mnd1.a* mutant plants.

Supplemental Figure S4. Duration of leaf and tiller outgrowth in *mnd1.a* mutant plants.

Supplemental Figure S5. Allelism crosses between the backcross-derived *mnd1.a* line and the putative *HvMND1* mutant lines *mbd* and MHOR198.

Supplemental Figure S6. Aerial shoot branching in *mbd*, *mnd1.a*, and MHOR198 mutants and in heterozygous F1 progeny of crosses *mbd* × *mnd1.a* and MHOR198 × *mnd1.a*.

Supplemental Figure S7. Maximum likelihood phylogenetic tree of acyl-CoA *N*-acyltransferase-like genes in 19 monocot and eudicot plant species.

Supplemental Figure S8. Diversity analysis of *HvMND1*.

Supplemental Figure S9. Corresponding negative controls of the *HvMND1* in situ hybridization experiment and *HvMND1* transcript localization in cv ZOH.

Supplemental Figure S10. Lys-acetylated proteins in young developing inflorescences (W3.5) in cv Bowman and *mnd1.a*.

Supplemental Figure S11. *HvMND1* expression determined by RT-qPCR.

Supplemental Figure S12. Principal-component analysis of DETs in cv Bowman and *mnd1.a*.

Supplemental Figure S13. Expression analysis of miR156-targeted *SQUAMOSA-promoter binding like* (*SPL*) genes in the *mnd1.a* mutant.

Supplemental Figure S14. Representation of leaf-enriched inflorescence tissue dissected for RNA extraction.

Supplemental Table S1. Phyllochron and plastochron of cv Bowman and *mnd1.a* mutant plants.

Supplemental Table S2. Nonsynonymous mutations assigned to a conserved domain of the corresponding protein in *mnd1.a* backcross-derived mutants identified through mapping by RNA sequencing.

Supplemental Table S3. Resequencing of candidate polymorphisms in the parental lines cv Bowman and cv Mesa, the backcross-derived *mnd1.a* mutant (*mnd1.a*), and the original *mnd1.a* mutant in cv Mesa [*mnd1.a* (M)].

Supplemental Table S4. Allelism test between *mnd1.a* and *mbd* mutants in the cv Bowman and cv ZOH genetic backgrounds, respectively.

Supplemental Table S5. Allelism test between *mnd1.a* and MHOR198 in the cv Bowman and cv HOR3069 genetic backgrounds, respectively.

Supplemental Table S6. Haplotypes of *HvMND1* and assignment of accessions carrying the *HvMND1* alleles.

Supplemental Table S7. Mutants used in this study.

Supplemental Table S8. Primer pairs used in this study.

Supplemental Dataset S1. Multiple sequence alignment of the *HvMND1* CDS.

Supplemental Dataset S2. Differentially expressed transcripts in developing *mnd1.a* mutant inflorescences.

ACKNOWLEDGMENTS

We cordially thank Thea Rütjes, Kerstin Luxa, Caren Dawidson, Andrea Lossow, and Rainer Franzen for excellent technical assistance, Jinshun Zhong for help with the construction of the phylogenetic tree, and Nils Stein for providing seed material of the MHOR198 mutant and critically reading this manuscript.

Received January 28, 2020; accepted April 19, 2020; published May 6, 2020.

LITERATURE CITED

Albani MC, Coupland G (2010) Comparative analysis of flowering in annual and perennial plants. Curr Top Dev Biol **91:** 323–348

Asbe A, Matsushita SC, Gordon S, Kirkpatrick HE, Madlung A (2015) Floral reversion in *Arabidopsis suecica* is correlated with the onset of flowering and meristem transitioning. PLoS One **10:** e0127897

Bartel DP (2009) MicroRNAs: Target recognition and regulatory functions. Cell **136:** 215–233

Bartlett ME, Thompson B (2014) Meristem identity and phyllotaxis in inflorescence development. Front Plant Sci **5:** 508

Bergonzi S, Albani MC, Ver E, Themaat LV, Wang R, Moerland PD, Coupland G (2013) Mechanisms of age-dependent response to winter temperature in perennial flowering of *Arabis alpina*. Science **340:** 1094–1098

Bi X, van Esse W, Mulki MA, Kirschner G, Zhong J, Simon R, von Korff M (2019) CENTRORADIALIS interacts with *FLOWERING LOCUS T*-like genes to control floret development and grain number. Plant Physiol **180:** 1013–1030

Bleckmann A, Weidtkamp-Peters S, Seidel CAM, Simon R (2010) Stem cell signaling in Arabidopsis requires CRN to localize CLV2 to the plasma membrane. Plant Physiol **152:** 166–176

Bommert P, Whipple C (2018) Grass inflorescence architecture and meristem determinacy. Semin Cell Dev Biol **79:** 37–47

Bonnet E, Wuyts J, Rouzé P, Van de Peer Y (2004) Detection of 91 potential conserved plant microRNAs in *Arabidopsis thaliana* and *Oryza sativa* identifies important target genes. Proc Natl Acad Sci USA **101:** 11511–11516

Bossinger G, Rohde W, Lundqvist U, Salamini F (1992) Genetics of barley development: Mutant phenotypes and molecular aspects. In P Shewry, ed, Barley: Genetics, Biochemistry, Molecular Biology, and Biotechnology. Oxford University Press, Oxford, pp 231–263

Bradley D, Carpenter R, Copsey L, Vincent C, Rothstein S, Coen E (1996) Control of inflorescence architecture in *Antirrhinum*. Nature **379:** 791–797

Bregitzer P, Lundqvist U, Franckowiak JD, Carollo Blake V (2014) Full descriptions of barley genetic stocks. Barley Genet Newsl **43:** 48–223

Buendía-Monreal M, Gillmor CS (2018) The times they are A-changin': Heterochrony in plant development and evolution. Front Plant Sci **9:** 1349

Campoli C, Drosse B, Searle I, Coupland G, von Korff M (2012) Functional characterisation of *HvCO1*, the barley (*Hordeum vulgare*) flowering time ortholog of *CONSTANS*. Plant J **69:** 868–880

Chen ZJ, Tian L (2007) Roles of dynamic and reversible histone acetylation in plant development and polyploidy. Biochim Biophys Acta **1769:** 295–307

Choi Y, Chan AP (2015) PROVEAN web server: A tool to predict the functional effect of amino acid substitutions and indels. Bioinformatics **31:** 2745–2747

Chuck G, Cigan AM, Saeteurn K, Hake S (2007) The heterochronic maize mutant *Corngrass1* results from overexpression of a tandem microRNA. Nat Genet **39:** 544–549

Cline M (1997) Concepts and terminology of apical dominance. Am J Bot **84:** 1064–1069

Cline MG (2000) Execution of the auxin replacement apical dominance experiment in temperate woody species. Am J Bot **87:** 182–190

Comadran J, Kilian B, Russell J, Ramsay L, Stein N, Ganal M, Shaw P, Bayer M, Thomas W, Marshall D, et al (2012) Natural variation in a homolog of *Antirrhinum CENTRORADIALIS* contributed to spring growth habit and environmental adaptation in cultivated barley. Nat Genet **44:** 1388–1392

Conklin PA, Strable J, Li S, Scanlon MJ (2019) On the mechanisms of development in monocot and eudicot leaves. New Phytol **221:** 706–724

Davies B, Schwarz-Sommer Z (1994) Control of floral organ identity by homeotic MADS-box transcription factors. In L Nover, ed, Plant Promoters and Transcription Factors. Springer, Berlin, Heidelberg, pp 235–258

Debernardi JM, Lin H, Chuck G, Faris JD, Dubcovsky J (2017) microRNA172 plays a crucial role in wheat spike morphogenesis and grain threshability. Development **144:** 1966–1975

Deshaies RJ, Joazeiro CA (2009) RING domain E3 ubiquitin ligases. Annu Rev Biochem **78:** 399–434

De Smet I, Voss U, Jürgens G, Beeckman T (2009) Receptor-like kinases shape the plant. Nat Cell Biol **11:** 1166–1173

Digel B, Tavakol E, Verderio G, Tondelli A, Xu X, Cattivelli L, Rossini L, von Korff M (2016) Photoperiod-H1 (Ppd-H1) controls leaf size. Plant Physiol **172:** 405–415

Dolzblasz A, Nardmann J, Clerici E, Causier B, van der Graaff E, Chen J, Davies B, Werr W, Laux T (2016) Stem cell regulation by *Arabidopsis WOX* genes. Mol Plant **9:** 1028–1039

Driessen HPC, de Jong WW, Tesser GI, Bloemendal H (1985) The mechanism of N-terminal acetylation of proteins. CRC Crit Rev Biochem **18:** 281–325

Druka A, Franckowiak J, Lundqvist U, Bonar N, Alexander J, Houston K, Radovic S, Shahinnia F, Vendramin V, Morgante M, et al (2011) Genetic dissection of barley morphology and development. Plant Physiol **155:** 617–627

Edgar RC (2004) MUSCLE: Multiple sequence alignment with high accuracy and high throughput. Nucleic Acids Res **32:** 1792–1797

Epstein E, Ludwig-Müller J (1993) Indole-3-butyric acid in plants: Occurrence, synthesis, metabolism and transport. Physiol Plant **88:** 382–389

Franckowiak JD, Lundqvist U, Konishi T (1996) New and revised descriptions of barley genes. Barley Genet Newsl **26:** 22–43

Gallavotti A (2013) The role of auxin in shaping shoot architecture. J Exp Bot **64:** 2593–2608

Goodstein DM, Shu S, Howson R, Neupane R, Hayes RD, Fazo J, Mitros T, Dirks W, Hellsten U, Putnam N, et al (2012) Phytozome: A comparative platform for green plant genomics. Nucleic Acids Res **40:** D1178–D1186

Götz S, García-Gómez JM, Terol J, Williams TD, Nagaraj SH, Nueda MJ, Robles M, Talón M, Dopazo J, Conesa A (2008) High-throughput functional annotation and data mining with the Blast2GO suite. Nucleic Acids Res **36:** 3420–3435

Guo T, Chen K, Dong NQ, Shi CL, Ye WW, Gao JP, Shan JX, Lin HX (2018) *GRAIN SIZE AND NUMBER1* negatively regulates the OSMKKK10-OSMKK4-OSMPK6 cascade to coordinate the trade-off between grain number per panicle and grain size in rice. Plant Cell **30:** 871–888

Gustafsson Å (1947) Mutations in agricultural plants. Hereditas **33:** 1–100

Harlan HV, Pope MN (1922) Many-noded dwarf barley. J Hered **13:** 269–273

Hartl M, König AC, Finkemeier I (2015) Identification of lysine-acetylated mitochondrial proteins and their acetylation sites. Methods Mol Biol **1305:** 107–121

Hayashi-Tsugane M, Maekawa M, Tsugane K (2015) A gain-of-function *Bushy dwarf tiller 1* mutation in rice microRNA gene *miR156d* caused by insertion of the DNA transposon *nDart1*. Sci Rep **5:** 14357

Hejátko J, Blilou I, Brewer PB, Friml J, Scheres B, Benková E (2006) In situ hybridization technique for mRNA detection in whole mount *Arabidopsis* samples. Nat Protoc **1:** 1939–1946

Hibara K, Isono M, Mimura M, Sentoku N, Kojima M, Sakakibara H, Kitomi Y, Yoshikawa T, Itoh J, Nagato Y (2016) Jasmonate regulates juvenile-to-adult phase transition in rice. Development **143:** 3407–3416

Hor KS (1924) Interrelations of genetic factors in barley. Genetics **9:** 151–180

Houston K, Druka A, Bonar N, Macaulay M, Lundqvist U, Franckowiak J, Morgante M, Stein N, Waugh R (2012) Analysis of the barley bract suppression gene Trd1. Theor Appl Genet **125:** 33–45

Huson DH, Scornavacca C (2012) Dendroscope 3: An interactive tool for rooted phylogenetic trees and networks. Syst Biol **61:** 1061–1067

Itoh JI, Hasegawa A, Kitano H, Nagato Y (1998) A recessive heterochronic mutation, plastochron1, shortens the plastochron and elongates the vegetative phase in rice. Plant Cell **10:** 1511–1522

Jeong JH, Song HR, Ko JH, Jeong YM, Kwon YE, Seol JH, Amasino RM, Noh B, Noh YS (2009) Repression of FLOWERING LOCUS T chromatin by functionally redundant histone H3 lysine 4 demethylases in Arabidopsis. PLoS One **4:** e8033

Jiang D, Yang W, He Y, Amasino RM (2007) *Arabidopsis* relatives of the human lysine-specific Demethylase1 repress the expression of *FWA* and *FLOWERING LOCUS C* and thus promote the floral transition. Plant Cell **19:** 2975–2987

Johnston R, Leiboff S, Scanlon MJ (2015) Ontogeny of the sheathing leaf base in maize (*Zea mays*). New Phytol **205:** 306–315

Kebrom TH, Spielmeyer W, Finnegan EJ (2013) Grasses provide new insights into regulation of shoot branching. Trends Plant Sci **18:** 41–48

Kernich GC, Halloran GM, Flood RG (1995) Variation in developmental patterns of wild barley (*Hordeum spontaneum* L.) and cultivated barley (*H. vulgare* L.). Euphytica **82:** 105–115

Keyte AL, Smith KK (2014) Heterochrony and developmental timing mechanisms: Changing ontogenies in evolution. Semin Cell Dev Biol **34:** 99–107

Kim JY, Oh JE, Noh YS, Noh B (2015) Epigenetic control of juvenile-to-adult phase transition by the Arabidopsis SAGA-like complex. Plant J **83:** 537–545

Kirschner GK, Stahl Y, Von Korff M, Simon R (2017) Unique and conserved features of the barley root meristem. Front Plant Sci **8:** 1240

Kobayashi K, Yasuno N, Sato Y, Yoda M, Yamazaki R, Kimizu M, Yoshida H, Nagamura Y, Kyozuka J (2012) Inflorescence meristem identity in rice is specified by overlapping functions of three *AP1/FUL*-like MADS box genes and *PAP2*, a *SEPALLATA* MADS box gene. Plant Cell **24:** 1848–1859

Kyozuka J, Tokunaga H, Yoshida A (2014) Control of grass inflorescence form by the fine-tuning of meristem phase change. Curr Opin Plant Biol **17:** 110–115

Lampropoulos A, Sutikovic Z, Wenzl C, Maegele I, Lohmann JU, Forner J (2013) GreenGate—a novel, versatile, and efficient cloning system for plant transgenesis. PLoS One **8:** e83043

Lehman A, Black R, Ecker JR (1996) *HOOKLESS1*, an ethylene response gene, is required for differential cell elongation in the *Arabidopsis* hypocotyl. Cell **85:** 183–194

Leigh JW, Bryant D (2015) POPART: Full-feature software for haplotype network construction. Methods Ecol Evol **6:** 1110–1116

Li C, Lin H, Chen A, Lau M, Jernstedt J, Dubcovsky J (2019) Wheat *VRN1*, *FUL2* and *FUL3* play critical and redundant roles in spikelet development and spike determinacy. Development **146:** dev175398

Li H (2013) Aligning sequence reads, clone sequences and assembly contigs with BWA-MEM. arXiv, https://arxiv.org/abs/1303.3997

Li J, Wang Z, Hu Y, Cao Y, Ma L (2017) Polycomb group proteins RING1A and RING1B regulate the vegetative phase transition in *Arabidopsis*. Front Plant Sci **8:** 867

Li P, Johnston MO (2000) Heterochrony in plant evolutionary studies through the twentieth century. Bot Rev **66:** 57–88

Liao CJ, Lai Z, Lee S, Yun DJ, Mengiste T (2016) *Arabidopsis* HOOKLESS1 regulates responses to pathogens and abscisic acid through interaction with MED18 and acetylation of *WRKY33* and *ABI5* chromatin. Plant Cell **28:** 1662–1681

Liller CB, Neuhaus R, von Korff M, Koornneef M, van Esse W (2015) Mutations in barley row type genes have pleiotropic effects on shoot branching. PLoS One **10:** e0140246

Liu J, Cheng X, Liu P, Sun J (2017) miR156-targeted SBP-box transcription factors interact with DWARF53 to regulate *TEOSINTE BRANCHED1*

and *BARREN STALK1* expression in bread wheat. Plant Physiol **174:** 1931–1948

Liu L, Li B, Liu X (2016) *FAR-RED ELONGATED HYPOCOTYL3* promotes floral meristem determinacy in *Arabidopsis*. Plant Signal Behav **11:** e1238545

Liu Q, Shen G, Peng K, Huang Z, Tong J, Kabir MH, Wang J, Zhang J, Qin G, Xiao L (2015) The alteration in the architecture of a T-DNA insertion rice mutant *osmtd1* is caused by up-regulation of *MicroRNA156f*. J Integr Plant Biol **57:** 819–829

Lu F, Cui X, Zhang S, Jenuwein T, Cao X (2011) Arabidopsis REF6 is a histone H3 lysine 27 demethylase. Nat Genet **43:** 715–719

Marchler-Bauer A, Derbyshire MK, Gonzales NR, Lu S, Chitsaz F, Geer LY, Geer RC, He J, Gwadz M, Hurwitz DI, et al (2015) CDD: NCBI's conserved domain database. Nucleic Acids Res **43:** D222–D226

Mascher M, Gundlach H, Himmelbach A, Beier S, Twardziok SO, Wicker T, Radchuk V, Dockter C, Hedley PE, Russell J, et al (2017) A chromosome conformation capture ordered sequence of the barley genome. Nature **544:** 427–433

Mascher M, Jost M, Kuon J-E, Himmelbach A, Aßfalg A, Beier S, Scholz U, Graner A, Stein N (2014) Mapping-by-sequencing accelerates forward genetics in barley. Genome Biol **15:** R78

Mayer KFX, Martis M, Hedley PE, Simková H, Liu H, Morris JA, Steuernagel B, Taudien S, Roessner S, Gundlach H, et al (2011) Unlocking the barley genome by chromosomal and comparative genomics. Plant Cell **23:** 1249–1263

McKenna A, Hanna M, Banks E, Sivachenko A, Cibulskis K, Kernytsky A, Garimella K, Altshuler D, Gabriel S, Daly M, et al (2010) The Genome Analysis Toolkit: A MapReduce framework for analyzing next-generation DNA sequencing data. Genome Res **20:** 1297–1303

McKim SM (2019) How plants grow up. J Integr Plant Biol **61:** 257–277

McKim SM, Koppolu R, Schnurbusch T (2018) Barley inflorescence architecture. In N Stein, and GJ Muehlbauer, eds, The Barley Genome. Springer, Cham, Switzerland, pp 171–208

McMaster GS (2005) Phytomers, phyllochrons, phenology and temperate cereal development. J Agric Sci **143:** 137–150

McSteen P, Leyser O (2005) Shoot branching. Annu Rev Plant Biol **56:** 353–374

Melzer S, Lens F, Gennen J, Vanneste S, Rohde A, Beeckman T (2008) Flowering-time genes modulate meristem determinacy and growth form in *Arabidopsis thaliana*. Nat Genet **40:** 1489–1492

Miyoshi K, Ahn B-O, Kawakatsu T, Ito Y, Itoh J, Nagato Y, Kurata N (2004) *PLASTOCHRON1*, a timekeeper of leaf initiation in rice, encodes cytochrome P450. Proc Natl Acad Sci USA **101:** 875–880

Müller-Xing R, Clarenz O, Pokorny L, Goodrich J, Schubert D (2014) Polycomb-group proteins and *FLOWERING LOCUS T* maintain commitment to flowering in *Arabidopsis thaliana*. Plant Cell **26:** 2457–2471

Müller D, Leyser O (2011) Auxin, cytokinin and the control of shoot branching. Ann Bot **107:** 1203–1212

Nakagawa M, Shimamoto K, Kyozuka J (2002) Overexpression of *RCN1* and *RCN2*, rice *TERMINAL FLOWER 1/CENTRORADIALIS* homologs, confers delay of phase transition and altered panicle morphology in rice. Plant J **29:** 743–750

Noh B, Lee SH, Kim HJ, Yi G, Shin EA, Lee M, Jung KJ, Doyle MR, Amasino RM, Noh YS (2004) Divergent roles of a pair of homologous jumonji/zinc-finger-class transcription factor proteins in the regulation of Arabidopsis flowering time. Plant Cell **16:** 2601–2613

Oikawa T, Kyozuka J (2009) Two-step regulation of *LAX PANICLE1* protein accumulation in axillary meristem formation in rice. Plant Cell **21:** 1095–1108

Pabón-Mora N, Di Stilio VS, Becker A (2019) Editorial: Genetic regulatory mechanisms underlying developmental shifts in plant evolution. Front Plant Sci **10:** 710

Patro R, Duggal G, Love MI, Irizarry RA, Kingsford C (2017) Salmon provides fast and bias-aware quantification of transcript expression. Nat Methods **14:** 417–419

Picó S, Ortiz-Marchena MI, Merini W, Calonje M (2015) Deciphering the role of POLYCOMB REPRESSIVE COMPLEX1 variants in regulating the acquisition of flowering competence in Arabidopsis. Plant Physiol **168:** 1286–1297

Pnueli L, Carmel-Goren L, Hareven D, Gutfinger T, Alvarez J, Ganal M, Zamir D, Lifschitz E (1998) The *SELF-PRUNING* gene of tomato regulates vegetative to reproductive switching of sympodial meristems and is the ortholog of *CEN* and *TFL1*. Development **125:** 1979–1989

Poethig RS (1988) Heterochronic mutations affecting shoot development in maize. Genetics **119:** 959–973

Poethig RS (2010) The past, present, and future of vegetative phase change. Plant Physiol **154:** 541–544

Preibisch S, Saalfeld S, Tomancak P (2009) Globally optimal stitching of tiled 3D microscopic image acquisitions. Bioinformatics **25:** 1463–1465

R Development Core Team (2011) R: A Language and Environment for Statistical Computing. R Found Stat Comput, Vienna

Rao NN, Prasad K, Kumar PR, Vijayraghavan U (2008) Distinct regulatory role for *RFL*, the rice *LFY* homolog, in determining flowering time and plant architecture. Proc Natl Acad Sci USA **105:** 3646–3651

Ratcliffe OJ, Amaya I, Vincent CA, Rothstein S, Carpenter R, Coen ES, Bradley DJ (1998) A common mechanism controls the life cycle and architecture of plants. Development **125:** 1609–1615

Rhoades MW, Reinhart BJ, Lim LP, Burge CB, Bartel B, Bartel DP (2002) Prediction of plant microRNA targets. Cell **110:** 513–520

Robinson D, Hayes A, Gomez M, Demeshev B, Menn D, Nutter B, Johnston L, Bolker B, Briatte F, Arnold J, et al (2018) Convert Statistical Analysis Objects into Tidy Tibbles. https://CRAN.R-project.org/package=broom

Rossini L, Muehlbauer GJ, Okagaki R, Salvi S, von Korff M (2018) Genetics of whole plant morphology and architecture. In N Stein, and GJ Muehlbauer, eds, The Barley Genome. Springer International Publishing, Cham, pp 209–231

Russell J, Mascher M, Dawson IK, Kyriakidis S, Calixto C, Freund F, Bayer M, Milne I, Marshall-Griffiths T, Heinen S, et al (2016) Exome sequencing of geographically diverse barley landraces and wild relatives gives insights into environmental adaptation. Nat Genet **48:** 1024–1030

Sadras VO (2007) Evolutionary aspects of the trade-off between seed size and number in crops. F Crop Res **100:** 125–138

Schindelin J, Arganda-Carreras I, Frise E, Kaynig V, Longair M, Pietzsch T, Preibisch S, Rueden C, Saalfeld S, Schmid B, et al (2012) Fiji: An open-source platform for biological-image analysis. Nat Methods **9:** 676–682

Schmitz G, Theres K (2005) Shoot and inflorescence branching. Curr Opin Plant Biol **8:** 506–511

Schwab R, Palatnik JF, Riester M, Schommer C, Schmid M, Weigel D (2005) Specific effects of microRNAs on the plant transcriptome. Dev Cell **8:** 517–527

Shannon S, Meeks-Wagner DR (1991) A mutation in the *Arabidopsis TFL1* gene affects inflorescence meristem development. Plant Cell **3:** 877–892

Si L, Chen J, Huang X, Gong H, Luo J, Hou Q, Zhou T, Lu T, Zhu J, Shangguan Y, et al (2016) OsSPL13 controls grain size in cultivated rice. Nat Genet **48:** 447–456

Smith LG, Hake S (1992) The initiation and determination of leaves. Plant Cell **4:** 1017–1027

Song XJ, Kuroha T, Ayano M, Furuta T, Nagai K, Komeda N, Segami S, Miura K, Ogawa D, Kamura T, et al (2015) Rare allele of a previously unidentified histone H4 acetyltransferase enhances grain weight, yield, and plant biomass in rice. Proc Natl Acad Sci USA **112:** 76–81

Stamatakis A, Hoover P, Rougemont J (2008) A rapid bootstrap algorithm for the RAxML Web servers. Syst Biol **57:** 758–771

Takeda S, Hanano K, Kariya A, Shimizu S, Zhao L, Matsui M, Tasaka M, Aida M (2011) CUP-SHAPED COTYLEDON1 transcription factor activates the expression of *LSH4* and *LSH3*, two members of the ALOG gene family, in shoot organ boundary cells. Plant J **66:** 1066–1077

Tamura K, Peterson D, Peterson N, Stecher G, Nei M, Kumar S (2011) MEGA5: Molecular evolutionary genetics analysis using maximum likelihood, evolutionary distance, and maximum parsimony methods. Mol Biol Evol **28:** 2731–2739

Teichmann T, Muhr M (2015) Shaping plant architecture. Front Plant Sci **6:** 233

Telles E, Seto E (2012) Modulation of cell cycle regulators by HDACs. Front Biosci (Schol Ed) **4:** 831–839

Tooke F, Ordidge M, Chiurugwi T, Battey N (2005) Mechanisms and function of flower and inflorescence reversion. J Exp Bot **56:** 2587–2599

Trevaskis B, Tadege M, Hemming MN, Peacock WJ, Dennis ES, Sheldon C (2007) *Short vegetative phase*-like MADS-box genes inhibit floral meristem identity in barley. Plant Physiol **143:** 225–235

Tripathi RK, Bregitzer P, Singh J (2018) Genome-wide analysis of the SPL/miR156 module and its interaction with the AP2/miR172 unit in barley. Sci Rep **8:** 7085

Vandenbussche M, Horstman A, Zethof J, Koes R, Rijpkema AS, Gerats T (2009) Differential recruitment of *WOX* transcription factors for lateral development and organ fusion in petunia and *Arabidopsis*. Plant Cell **21:** 2269–2283

van Esse GW, Walla A, Finke A, Koornneef M, Pecinka A, von Korff M (2017) Six-Rowed Spike3 (VRS3) is a histone demethylase that controls lateral spikelet development in barley. Plant Physiol **174:** 2397–2408

Vierstra RD (2009) The ubiquitin-26S proteasome system at the nexus of plant biology. Nat Rev Mol Cell Biol **10:** 385–397

Waddington SR, Cartwright PM, Wall PC (1983) A quantitative scale of spike initial and pistil development in barley and wheat. Ann Bot **51:** 119–130

Wang B, Smith SM, Li J (2018) Genetic regulation of shoot architecture. Annu Rev Plant Biol **69:** 437–468

Wang H, Wang H (2015) Multifaceted roles of *FHY3* and *FAR1* in light signaling and beyond. Trends Plant Sci **20:** 453–461

Weigel D, Alvarez J, Smyth DR, Yanofsky MF, Meyerowitz EM (1992) *LEAFY* controls floral meristem identity in *Arabidopsis*. Cell **69:** 843–859

Wenzel CL, Chandler PM, Cunningham RB, Passioura JB (1997) Characterization of the leaf epidermis of barley (*Hordeum vulgare* L. 'Himalaya'). Ann Bot **79:** 41–46

Whipple CJ (2017) Grass inflorescence architecture and evolution: The origin of novel signaling centers. New Phytol **216:** 367–372

Whipple CJ, Kebrom TH, Weber AL, Yang F, Hall D, Meeley R, Schmidt R, Doebley J, Brutnell TP, Jackson DP (2011) *grassy tillers1* promotes apical dominance in maize and responds to shade signals in the grasses. Proc Natl Acad Sci USA **108:** E506–E512

Wu F, Shi X, Lin X, Liu Y, Chong K, Theißen G, Meng Z (2017) The ABCs of flower development: Mutational analysis of *AP1/FUL*-like genes in rice provides evidence for a homeotic (A)-function in grasses. Plant J **89:** 310–324

Wu G, Park MY, Conway SR, Wang JW, Weigel D, Poethig RS (2009) The sequential action of miR156 and miR172 regulates developmental timing in *Arabidopsis*. Cell **138:** 750–759

Wu X, Chory J, Weigel D (2007) Combinations of *WOX* activities regulate tissue proliferation during *Arabidopsis* embryonic development. Dev Biol **309:** 306–316

Xie K, Wu C, Xiong L (2006) Genomic organization, differential expression, and interaction of SQUAMOSA promoter-binding-like transcription factors and microRNA156 in rice. Plant Physiol **142:** 280–293

Xu C, Wang Y, Yu Y, Duan J, Liao Z, Xiong G, Meng X, Liu G, Qian Q, Li J (2012) Degradation of MONOCULM 1 by APC/C^{TAD1} regulates rice tillering. Nat Commun **3:** 750–759

Xu M, Leichty AR, Hu T, Poethig RS (2018) H2A.Z promotes the transcription of *MIR156A* and *MIR156C* in *Arabidopsis* by facilitating the deposition of H3K4me3. Development **145:** dev152868

Yang C, Ma Y, He Y, Tian Z, Li J (2018) OsOFP19 modulates plant architecture by integrating the cell division pattern and brassinosteroid signaling. Plant J **93:** 489–501

Yoshida A, Sasao M, Yasuno N, Takagi K, Daimon Y, Chen R, Yamazaki R, Tokunaga H, Kitaguchi Y, Sato Y, et al (2013) *TAWAWA1*, a regulator of rice inflorescence architecture, functions through the suppression of meristem phase transition. Proc Natl Acad Sci USA **110:** 767–772

Youssef HM, Eggert K, Koppolu R, Alqudah AM, Poursarebani N, Fazeli A, Sakuma S, Tagiri A, Rutten T, Govind G, et al (2017) VRS2 regulates hormone-mediated inflorescence patterning in barley. Nat Genet **49:** 157–161

Zhang J (1997) Chromosome location of the gene for multinode, branched and dwarf syndrome mutation in barley. Hereditas **19:** 17–20

Zhang X, Clarenz O, Cokus S, Bernatavichute YV, Pellegrini M, Goodrich J, Jacobsen SE (2007) Whole-genome analysis of histone H3 lysine 27 trimethylation in Arabidopsis. PLoS Biol **5:** e129

Zhu QH, Upadhyaya NM, Gubler F, Helliwell CA (2009) Over-expression of miR172 causes loss of spikelet determinacy and floral organ abnormalities in rice (*Oryza sativa*). BMC Plant Biol **9:** 149